47TH TURBOMACHINERY & 34TH PUMP SYMPOSIA
HOUSTON, TEXAS | SEPTEMBER 17-20, 2018
GEORGE R. BROWN CONVENTION CENTER

LEAKAGE AND FORCE COEFFICIENTS FOR PUMP ANNULAR SEALS OPERATING WITH AIR/OIL MIXTURES: MEASUREMENTS VS PREDICTIONS AND AIR INJECTION TO INCREASE SEAL DYNAMIC STIFFNESS

Luis San Andrés
Mast-Childs Chair Professor
Lsanandres@tamu.edu

Xueliang Lu
Graduate Research Assistant
luliang413@gmail.com

Zhu Jie
Chief Engineer
zhuj@hnsund.com

Turbomachinery Laboratory
Texas A&M University
College Station, TX 77845-312

Hunan SUND Industrial & Technological Co., Ltd,
Xiangtan, HN, PR China 411101

Luis San Andrés performs research in lubrication and rotordynamics, having produced advanced technologies of hydrostatic bearings for primary power cryogenic turbo pumps, squeeze film dampers for aircraft jet engines, and gas foil bearings for oil-free micro turbomachinery. Luis is a Fellow of ASME and STLE, and a member of the Industrial Advisory Committees for the Texas A&M Turbomachinery Symposia. Dr. San Andrés has educated dozens of graduate students serving the profession with distinction. Dr. San Andrés earned a MS in ME from the University of Pittsburgh and a PhD in ME from Texas A&M University. Luis has published over 165 peer reviewed papers in various journals (ASME Journal of Tribology and ASME Journal of Engineering for Gas Turbines and Power). Several papers are recognized as best in various international conferences.

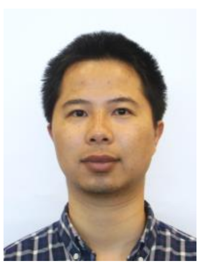

Xueliang Lu received his B.S. and M.S. degrees in Mechanical Engineering from Xiangtan University in China. After graduation, he joined the technical department of Hunan Sund Industrial and Technological Co. Ltd (2013-2014) (PR China) as a bearing design engineer. In 2014, Xueliang began pursuing a Ph.D. degree under the guidance of Dr. San Andrés at Texas A&M University and expects to complete his degree in 2018. Xueliang's research mainly focuses on the experimental identification and prediction of force coefficients for two phase flow annular seals and fluid film bearings. In June 2017, the Structures and Dynamics Division of ASME-Turbo Expo recognized one of his papers, co-authored with Dr. San Andrés, as best in the field.

Zhu Jie is the Chief Engineer of Hunan Sund Industrial and Technology Company in Hunan Province, PR China. He has over 10 years' experience with hydrodynamic bearings and seals, and has published more than 10 papers and holds 50 patents. Zhu Jie received his B.S degree from Chang'an Universtiy in 2004 and M.S degree from Xi'an Jiaotong University in 2007, both in the field of Mechanical Engineering. He is a member of SAC/TC 236 and joined the Asia Turbomachinery Symposium Advisory Committee in 2014.

ABSTRACT[1]

In the subsea oil and gas industry, multiphase pumps enable a long distance tie back system and eliminate topside oil and gas separation station. A persistent challenge to operate (vertical) centrifugal pumps handling (gas in liquid) mixtures is their poor reliability due to persistent sub synchronous vibrations. The mixture gas volume fraction (GVF), surely changing over time, affects the dynamic forced performance of leakage flow components, namely seals, and which may lead to an increase in lateral and axial rotor vibrations.

The lecture presents measurements of leakage and dynamic force coefficients for six annular seals (L = 46 mm, D = 127 mm) operating with an air in oil mixture ranging from pure liquid to just air. Each seal has a distinct clearance configuration: one is a plain seal with a small radial clearance (c_r=0.203 mm), and another has a larger (worn) clearance (c_r=0.274 mm); a third seal introduces a wavy clearance (c_m= 0.191 mm) that produces a significant centering stiffness; a fourth seal has a shallow groove pattern (c_r=0.211 mm); and the fifth and sixth seals have a stepped clearance (narrow to wide and wide to narrow).

1 This lecture extends the work in Ref. [1] presented at ATPS (2018).

At a shaft speed of 3.5 krpm (58 Hz), an air in ISO VG 10 oil mixture, GVF varying discretely from 0.0 to 0.9, feeds a test seal at a supply pressure P_s of 2.5 bar(a). The recorded mixture mass flow rate decreases continuously with an increase in inlet GVF. Dynamic loads excite the test seal with a small whirl amplitude and frequency ranging from ω =10 – 150 Hz. The seals operating with a pure liquid (GVF=0) show frequency independent force coefficients. On the other hand, operation with a mixture produces direct stiffness (K) and cross-coupled stiffness (k) that vary greatly with frequency, in particular K hardens with excitation frequency. The direct damping (C) coefficients, on the other hand, are not functions of excitation frequency, albeit dropping rapidly in magnitude as the GVF increases.

The test three-wave seal produces the greatest K and C, as well as the largest effective damping coefficient (C-k/ω). The worn surface (largest clearance) seal produces the smallest force coefficients and leaks the most. Operation with a large GVF produces little damping, albeit more than predicted. For all the test seals, the whirl frequency ratio (WFR) is around 50%. A step clearance seal, one with the narrow clearance facing the incoming flow, produces a significant negative direct stiffness (K<0) that could easily impact the static stability of a pump as it reduces its natural frequency. The magnitude of K increases with the supplied flow or supply pressure to exacerbate the issue. On the other hand, the other step clearance seal, one with a wide to narrow clearance, produces a positive direct stiffness. The other force coefficients (k,C, and M) are virtually identical for both stepped seals.

The multiple tests in a plain seal supplied with gas injection (GVF~0→0.6) in the oil stream demonstrate the seal recovers its dynamic stiffness, hence its usage to promote rotor stability in large hydraulic pump/turbine systems. Incidentally, one should realize that air injection reduces simultaneously the direct damping (C) and cross coupled dynamic stiffness (k), hence the WRF is still ~0.50. Air injection into a liquid stream causes a dramatic reduction in the mixture sound speed to make it highly compressible; hence the hardening of the seal direct stiffness (or reduction) of its added mass.

Predictions of seal force coefficients derived from a bulk flow model match well the test data for operation with a pure oil and a small GVF ~ 0.2. The discrepancy between the prediction and test data increases for operation with a larger gas content, GVF > 0.2. The comprehensive test campaign reveals the salient characteristics of certain annular seal configurations, thus aiding to better design multiple-phase flow centrifugal pumps.

INTRODUCTION

Centrifugal pumps rely on non-contacting annular seals to reduce leakage flows along their flow path to maintain high processing efficiency. Besides reducing leakage, the fluid confined in the small annular leakage path produces significant reaction forces that influence the placement of shaft critical speeds, thus affecting the rotor-bearing system synchronous imbalance response and its stability [2, 3]. Fig. 1 shows a cross section view of one stage for an electric submersible pump (ESP) with four (non-contacting) annular seals [4]. The main flow ① enters the impeller on the left and proceeds to the next stage through the diffuser on the right. As the fluid flows from left to the right, the pressure gradually increases. In a pump stage, there are four leakage flow paths: one is through the front wear ring seal ② formed by the outside diameter (OD) of the front shroud of the impeller and the inside diameter (ID) of the housing, another through the rear wear ring seal ③ between the impeller backside and the diffuser, a third flow crosses the inter stage insert seal ④ between the diffuser and the shaft. The leakage leaving the inter stage seal ④ then flows through the impeller insert seal to enter the back side of the upstream impeller.

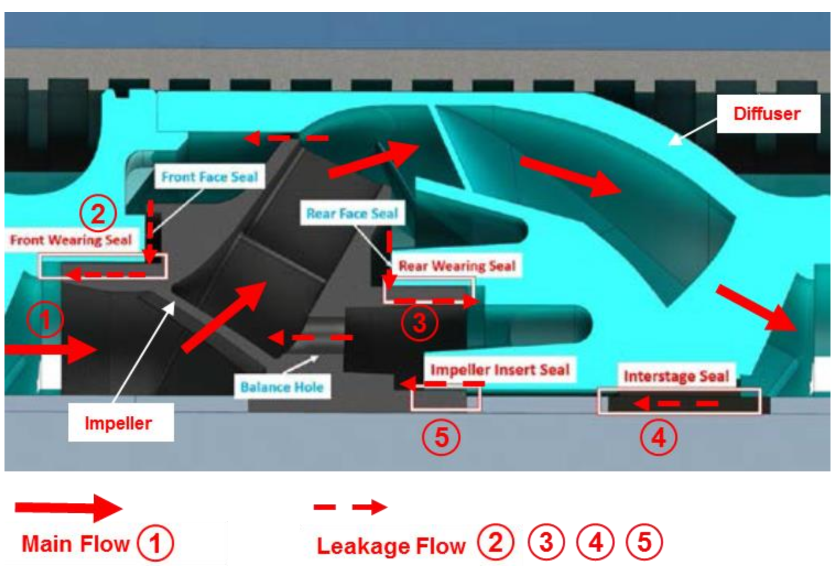

Fig. 1 Cross section view of one stage in an electrical submersible pump.
Adapted from Childs et al. [4] with permission.

In a centrifugal pump the total pressure rise (ΔP) across a pump stage is proportional to shaft speed squared (ΔP~Ω^2), and annular seals must restrict the leakage (Q) forced by an ever increasing ΔP, hence tight clearances are a norm. For an ESP running at a nominal rated speed of 3,600 rpm (60 Hz), the typical static ΔP for the front and rear wear ring seals is ~1.5 bar, whereas for the inter stage seal static ΔP is ~ 2.5 bar [4]. Typical annular seals utilized in centrifugal pumps vary in configuration; they can be smooth surface (plain) cylindrical seals, or stepped clearance seals, or grooved seals; all geometries aiming to reduce leakage with a low cost of manufacturing [5,6].

Although similar in geometry to plain journal bearings, annular seals generate a centering stiffness (K) through a different mechanism and even without shaft rotation. Figure 2 shows the typical geometry of an annular pressure seal [7] where the process fluid at high pressure (P_s) enters the annular seal clearance (c_r), flows through the seal film land, and discharges to an exit pressure (P_a). L and D denote the seal length and diameter, respectively. At the seal inlet plane with a sharp contraction in geometry, the stagnant process fluid upstream of the seal accelerates to produce a sharp change in the pressure at the seal entrance o inlet plane,

$$P_e = P_s - \tfrac{1}{2}\,\rho\,(1+\zeta)\,V_z^2 \tag{1}$$

above ρ is the fluid density, V_z is the bulk-flow axial velocity, and ζ is an (empirical) pressure loss coefficient, ranging from 0.0 to 0.60 [7].

In Fig. 2, an upward rotor motion (dashed line) causes the seal top clearance to reduce and the bottom clearance to increase. Consequently, the seal side with a small clearance has a larger flow resistance than for the flow on the side with a large clearance. Thus a smaller velocity (V_z) flows through the upper clearance, and Eq. (1) produces a lower pressure drop at the inlet. The opposite happens at the seal inlet in the bottom clearance. The pressure difference between the top and bottom clearances produces a reaction force that is opposite to the rotor displacement, thus creating a centering (positive) stiffness. The above mechanism is known as the Lomakin effect [7].

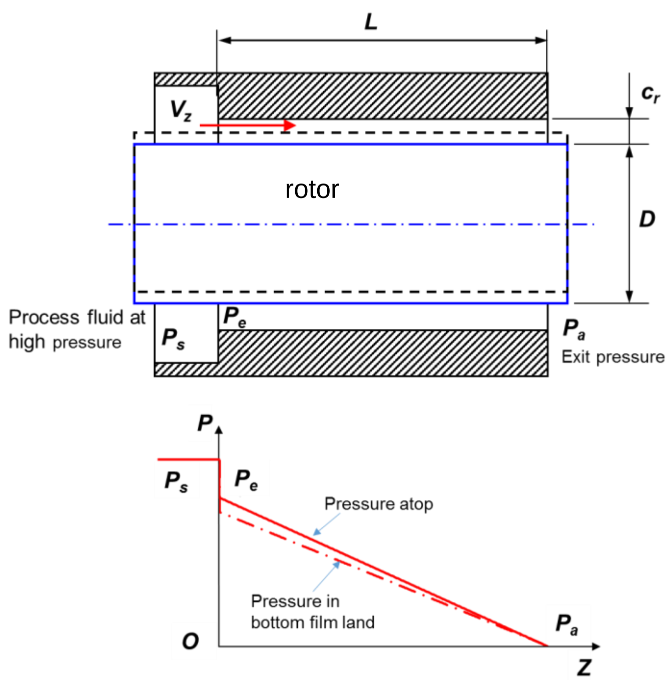

Fig. 2 Geometry of an annular seal and its pressure profile showing a sudden pressure drop at the seal entrance [7].

Annular seals produce a reaction force (**F**) due to shaft displacements $\mathbf{z}=\{x_{(t)}, y_{(t)}\}^T$. The typical linearized model is

$$\mathbf{F} = \begin{Bmatrix} F_X \\ F_Y \end{Bmatrix} = -\mathbf{K}\,\mathbf{z} - \mathbf{C}\,\dot{\mathbf{z}} - \mathbf{M}\,\ddot{\mathbf{z}} = -\begin{bmatrix} K_{XX} & K_{XY} \\ K_{YX} & K_{YY} \end{bmatrix}\begin{Bmatrix} x \\ y \end{Bmatrix} - \begin{bmatrix} C_{XX} & C_{XY} \\ C_{YX} & C_{YY} \end{bmatrix}\begin{Bmatrix} \dot{x} \\ \dot{y} \end{Bmatrix} - \begin{bmatrix} M_{XX} & M_{XY} \\ M_{YX} & M_{YY} \end{bmatrix}\begin{Bmatrix} \ddot{x} \\ \ddot{y} \end{Bmatrix} \tag{2}$$

The matrices **K, C** and **M** contain the stiffness, damping and inertia force coefficients, respectively. Fluid inertia or added mass coefficients (**M**) are significant in seals with dense fluids, which are liquids. In general, the force coefficients for liquid seals are frequency independent; and thus, the physical **K-C-M** model is adequate. However, operation with a gas or a gas in liquid mixture leads to direct stiffnesses that grow (or harden) with excitation frequency (ω) while damping drops, dramatically! Hence, $\mathbf{K}=\mathbf{K}_{(\omega)}$ and $\mathbf{C}=\mathbf{C}_{(\omega)}$ becomes more appropriate. This formulation includes the simple model $\mathbf{K}_{(\omega)}=\mathbf{K}-\omega^2\mathbf{M}$.

Lastly, for an axisymmetric seal and rotor motions about a centered condition, the direct force coefficients are identical, whereas the cross-coupled coefficients are opposite in sign, i.e. $K_{XX} = K_{YY} = K$, and $K_{XY} = -K_{YX} = k$, for example. Eq. (1) reduces to

$$\begin{Bmatrix} F_X \\ F_Y \end{Bmatrix} = -\begin{bmatrix} K_{(\omega)} & k_{(\omega)} \\ -k_{(\omega)} & K_{(\omega)} \end{bmatrix} \begin{Bmatrix} x \\ y \end{Bmatrix} - \begin{bmatrix} C_{(\omega)} & c_{(\omega)} \\ -c_{(\omega)} & C_{(\omega)} \end{bmatrix} \begin{Bmatrix} \dot{x} \\ \dot{y} \end{Bmatrix} \tag{3}$$

For circular centered motions with amplitude r and frequency ω, then $x = r\cos(\omega t), y = r\sin(\omega t), \ \dot{x} = -\omega y, \dot{y} = \omega x$; and the representation of the seal reaction force reduces to

$$\begin{Bmatrix} F_X \\ F_Y \end{Bmatrix} = -\left(K_{(\omega)} + \omega c_{(\omega)}\right) \begin{Bmatrix} x \\ y \end{Bmatrix} - \left(C_{(\omega)} - \tfrac{1}{\omega} k_{(\omega)}\right) \begin{Bmatrix} \dot{x} \\ \dot{y} \end{Bmatrix} \tag{4}$$

Above, $C_{eff}=C-k/\omega$ is an effective damping coefficient. $C_{eff}>0$ for the seal to be a stabilizing mechanical element.

San Andrés [7, 8] fully details a bulk-flow model (BFM), first originated by Hirs [9], for the prediction of the leakage and dynamic force coefficients of annular seals lubricated with single phase flow. As noted earlier, in a deep sea application, pumps have to withstand a gas-liquid mixture whose gas volume fraction (GVF) varies over a wide range (0 to 1) [10]. To bridge the gap between pressing industrial needs and predictive tools, San Andrés (2010) [11] and Arghir et al. (2011) [12] developed homogenous-mixture bulk flow models (BFM) to deliver the leakage and dynamic force coefficients of annular seals, including those with a textured stator surface. In general, the models predict a seal leakage, direct damping and drag power loss that decrease steadily with an increase in GVF. The other seal force coefficients also decrease with a large GVF; however the direct stiffness (K) may increase for small GVFs. In a liquid seal, the dynamic stiffness $K_{(\omega)}$**=(**K- $\omega^2 M$**)** decreases quickly with frequency (ω) as the added mass (M) coefficient is large for fluids with a large density. Arghir et al. also note that changes in GVF from 1% to 10% can produce frequency dependent force coefficients.

To date there is scant test programs producing reliable experimental results – leakage and force coefficients – for seals operating with multiple phase fluids. Many observations are anecdotal, with only a handful of papers reporting credible (reliable) results. Iwatsubo and Nishino (1993) [13] report force coefficients for a pump seal supplied with an air-water mixture whose gas volume fraction (GVF) varied from 0 (no gas) to 0.70. The seal has diameter D =70 mm, length L = 70 mm and radial clearance c = 0.5 mm, and operating at a shaft speed of 3,500 rpm (surface speed ΩR = 13 m/s) and a pressure drop 588 kPa (85 psi). Both measured radial and tangential components of the seal reaction force decrease steadily with an increase in GVF. The authors also report of a random vibration due to the two-phase flow, and that becomes large in magnitude for operation at GVF = 0.7.

In recent years, the deep sea oil and gas flow separation industry prompted research on *wet* annular seals, i.e., flows with a fraction of liquid in a main gas steam. Brenne et al. (2005) [14] measured the performance of a single stage compressor operating with a natural gas with up to just 3% hydrocarbon liquid volume fraction (LVF). Severe sub-synchronous rotor lateral vibrations (SSV) with ~0.5X frequency occurred when the LVF at the compressor suction side increased to 3%. The compressor balance piston is a long labyrinth seal. The authors suspect that trapped liquid in the labyrinth seal caused the SSV.

During a shop test with a two stage centrifugal compressor operating with a water in air mixture, Vannini et al. (2014) [15] recorded severe rotor SSV at 0. 45X in. A LVF as small as 0.5% could trigger the harmful SSV. After replacing the labyrinth seal balance piston with a pocket damper seal, the amplitude of the SSV dropped from 20 μm to just a few microns [16].

The late 2000's planned advent of emerging subsea factories prompted research at the Turbomachinery Laboratory. Childs and students [17] tackled *wet* seals for compressors and measured seal rotordynamic force coefficients that vary significantly with the liquid content in the gas stream. During the tests, conducted with air in silicon oil mixture with LVF $\leq$ 8%, the pressure drop across the seal is as large as 62 bar and the shaft speed is 20 krpm (ΩR = 96 m/s). The flow across the seal is mainly turbulent.

In a companion test program funded by the Turbomachinery Research Consortium (TRC), San Andrés and students [18-19] (2014-date) completed extensive research to quantify the influence of GVF on the leakage and dynamic forced performance of *bubbly* and *wet* annular seals, more applicable to pump conditions handling a largely viscous fluid (thick oil). This lecture reports the findings for six test seals, compares their performance, and thus provides design references for multiphase pumps.

DESCRIPTION OF TEST RIG, FLOW LOOP, AND TEST SEALS

Figure 3 shows an isometric view of the seal test rig and the coordinate system (X, Y) for reference of the seal housing displacements. Four flexible support rods (90° apart), with a total lateral stiffness K_s and structural damping coefficient C_s, connect the seal housing to a massive steel base. Two orthogonally mounted electromagnetic shakers, max. 440 N (100 lb_f) each, deliver dynamic loads via stingers to the seal housing and produce dynamic displacements for force coefficients. Note the test rig is designed such that the mass center of the assembled seal housing resides on the plane of the (X, Y) axes.

Table 1 lists the main dimensions for the test seal housing and fluid (air and ISO VG 10 oil)[2] physical properties. The test seals have a diameter (D) 127 mm and a length (L) 46 mm (max.), their nominal radial clearance ranging from 0.108 mm to 0.274 mm. Note the vast difference between the density and viscosity for the two individual fluid components.

2 The selected viscosity uses available lubricant in the laboratory. In an oil well the fluid viscosity could range from 800 cp (thick crude) to 1 cp (water-like), and changing as the oil field depletes.

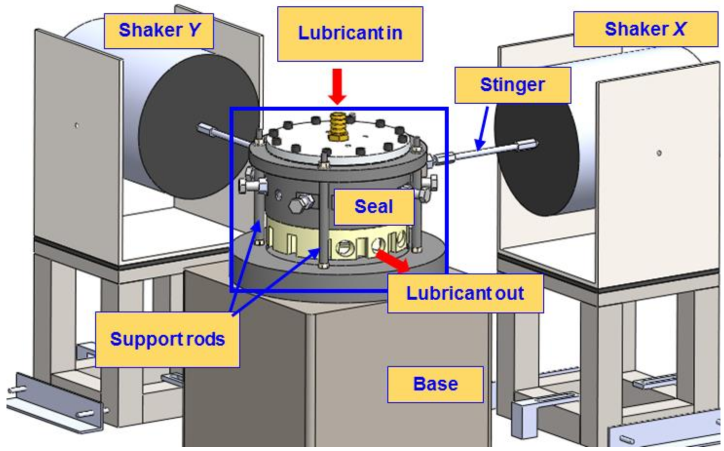

Fig. 3 Isometric view of seal test rig with shakers and lubricant supply line

Table 1. Dimensions of test seals and fluids physical properties.

ρ_l/ρ_{ga} = 728, μ_l/μ_{ga} = 530

Diameter, $D = 2R$	127 mm
Length, L	46 mm
Radial clearance, c	0.191 to 0.274 mm
ISO VG 10 viscosity, μ_l	10.1 cP (at 37 ºC)
Density, ρ_l	830 kg/m^3
Air viscosity, μ_{ga}	0.019 cP (at 37 ºC)
Density, ρ_{ga}	1.14 kg/m^3 at P_a = 1 bara
Max test supply & discharge pressures	3.5 bara, 1 bara
Top journal speed, $\Omega_{\max}$	3.5 krpm
Rotor surface speed, ½$D\Omega_{\max}$	23.3 m/s

Figure 4(a) shows a cross section view of the seal assembly with the lubricant flow path. The narrow gap between the inner diameter (ID) of a test element and the outside diameter (OD) of a rotating journal makes the lubricant seal section with a thin film land. A DC motor, through a transmission belt with a gear ratio of 1.8, drives the shaft and journal. The shaft supported on two rigid ball bearings (the graph only shows the top one), can spin to a maximum speed of 6 krpm (surface speed $R\Omega_{\max}$= 40 m/s).

The arrangement allows easy exchange of a test seal element without disassembling the entire mechanical structure. A seal element is installed inside a housing whose ID is 3 mm larger than the OD of the seal. Figure 4(b), cross section A-A, details the seal installation inside the housing. Four sets (2 bolts each) of centering bolts, 20˚ apart, inserted in the housing allow radial adjustment of the seal element. During the centering process, a feeler gauge measures the clearance (c) between the journal and the seal. After the seal is centered, a top lid with a bottom surface contacting the top surface of the seal element presses it against the seal housing.

The arrows in Fig. 4(a) denote the flows path through a seal. The mixture enters a plenum atop the seal housing with pressure P_s, and then flows through the seal annular clearance, to exit into an oil collection cup at ambient pressure, P_a=1 bara. Figure 5 depicts the fluids circulation system that consists of an air supply line drawing dry air from a large pressurized tank, and a gear pump and oil supply line that delivers ISO VG 10 oil at a constant volumetric flow rate. Needle valves control the air flow rate and the oil flow rate. An air mass flow meter measures the air volumetric flow rate (Q_{ga}) at a standard condition (20 ºC and 1 bara), and an oil turbine flow meter records the oil volumetric flow rate (Q_l). Both fluid streams merge into a sparger element with pore size of 2 μm to make an air in oil mixture. By regulating the needle valves, the system operator can make mixtures with any inlet GVF (0 → 1) or liquid volume fraction (LVF = 0 → 1). The actual GVF[3] at the seal inlet is

$$\mathrm{GVF}\Big|_{inlet} = \frac{Q_{ga}(P_a / P_s)}{Q_l + Q_{ga}(P_a / P_s)} \tag{5}$$

and the inlet gas mass fraction (GFM) is

[3] For a mixture where the ratio of liquid/gas densities >> 1, the liquid mass fraction (LMF) ~ 1 even for GVFs as large as 0.7, for example. Hence the GVF characterizes well the operation of multiple phase pumps as the volumetric flow rate does not change dramatically. On the other hand, for mixtures with (say) GVF>0.8, the liquid mass fraction (LMF) best characterizes wet gas compressors as it allows ready differentiation.

$$\mathrm{GMF} = \frac{\mathrm{GVF} \cdot \rho_{ga} \cdot (P_s / P_a)}{\mathrm{GVF} \cdot \rho_{ga} \cdot (P_s / P_a) + (1 - \mathrm{GVF}) \cdot \rho_l} \tag{6}$$

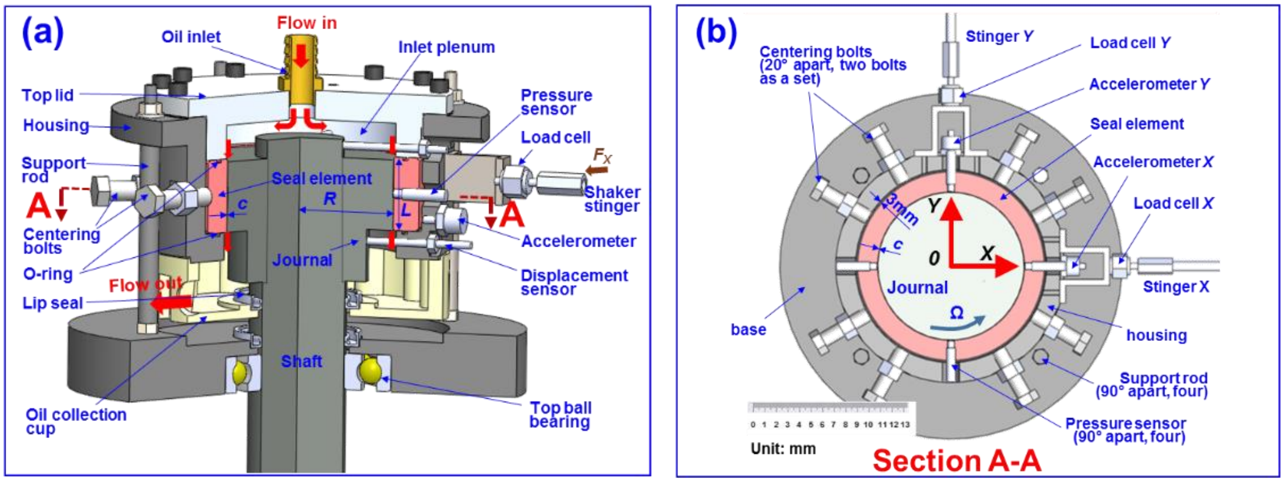

Fig. 4 (a) Cut view of test seal assembly with flow path, (b) section A-A with seal installed in housing.

Notice that since the gas density (ρ_{ga}) << liquid density (ρ_l), the GMF <<< GVF. In addition, LMF=1-GMF.

For large GVFs, the mixture exits the seal as a fog or mist. The return stream, forced by a gear pump, passes first through a bubble eliminator where most air bubbles are removed, to later fill a large oil tank while slowly flowing underneath a division wall. On one side of the tank any remnant dissolved gas is released; while the oil, having a higher density than the mixture, displaces to fill the other side of the tank. The lubricant physical properties (density and viscosity) are measured periodically to quantify any change due to gas entrainment.

During the dynamic load tests, two load cells installed on the seal housing record the applied loads. Four eddy current sensors and two piezoelectric accelerometers record the ensuing seal housing motions and accelerations. A data acquisition system records voltage signals from sensors at a rate of 12.8 k samples/s and the acquisition time lasts typically 10.2 s. Other instrumentation includes static and dynamic pressure sensors, and flow meters for both the oil and air streams.

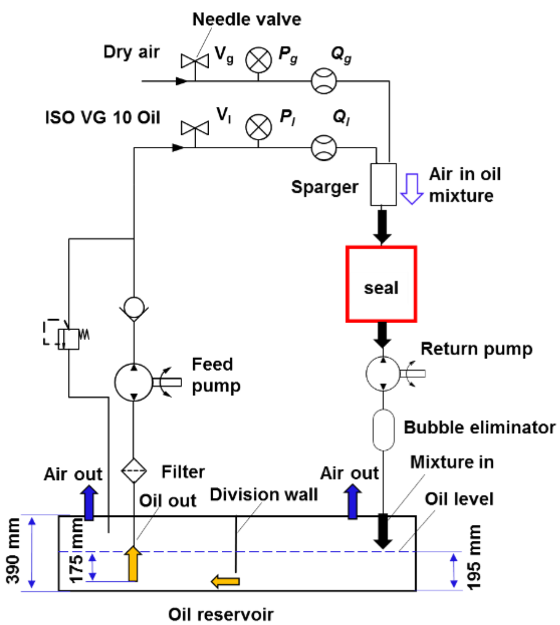

Fig. 5 Air and lubricant circulation flow systems.

The test seals

Figure 6 depicts schematic views of the test seals, all having the same length (L) and diameter (D). Each seal has a distinct clearance configuration: one is a plain seal (#1) with a small clearance (c=0.203 mm); another (#2) has a larger clearance (c=0.274 mm) as if worn out; and a third seal (#3) introduces a three-wave clearance (c_m= 0.191 mm). This wavy seal, with minimum and maximum clearances equal to 0.108 mm and 0.274 mm, is thought to produce a centering stiffness, a major benefit to vertical pumps that operate radially unloaded, thus raising their critical speed and enhancing rotor dynamic stability. The fourth seal (#4) with c=0.21 mm has 14 shallow grooves, each 1.5 mm long and a depth/clearance ratio d_g/c_r=2.6. The fifth and six seals have a step clearance (c_{min}=0.174 mm and c_{max}=0.274 mm), narrow to wide for seal #5, and wide to narrow for seal #6, respectively. The length of the small clearance section ranges between 10% and 20% of the seal overall length.

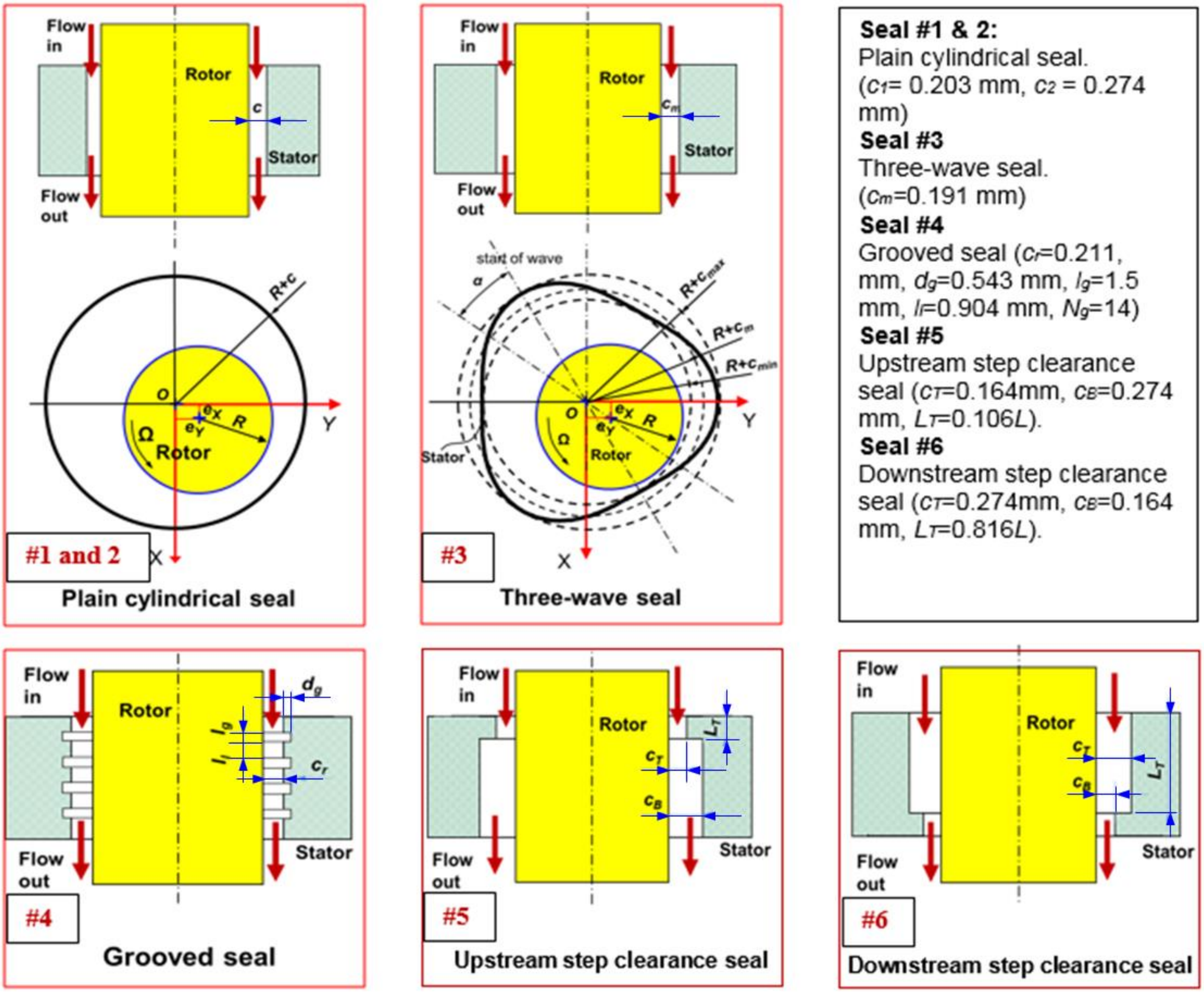

Fig. 6 Schematic views of six test seals: plain, wavy, grooved and stepped configurations.
Clearances exaggerated to illustrate the seal geometries.

EXAMPLES OF FLOW VISUALIZATION WITH PLAIN SEAL #1

An early seal housing was made of Plexiglas for visualization of the air-oil mixture flowing through the seal. Figure 7 displays videos for the air in oil mixture flowing through the thin film annulus and without shaft rotation. The videos are taken with a stroboscope light with frequency = 30 Hz, and are recorded at 60 frames/s. In each video, the mixture enters the seal on the top and flows downwards to exit the seal clearance on the bottom. As the videos show, most of the air bubbles travel separately for operation with inlet GVF < 0.7. For operation with larger inlet GVFs, some of the air bubbles coalesce. Note that although the sparger element makes bubbles 2 μm in size, by the time the mixture reaches the seal, the bubbles are large in size, much larger than the film clearance (c).

Figure 8 shows the air-oil mixture with an inlet GVF of 0.9 and operation with shaft angular speed at 1.8 krpm ($R\Omega$=12 m/s). The stroboscope light at 30 Hz freezes the shaft motion. In general, with a spinning shaft, individual air bubbles shown in Figure 7 vanish. Instead, the air bubbles coalesce to form air striations or fingering. The remnant air bubbles in the mixture, the ones small in size, mix uniformly with the oil to generate a milky effluent. Note the visualization shows the mixture is not homogeneous, suggesting the liquid and gas travel at different speeds.

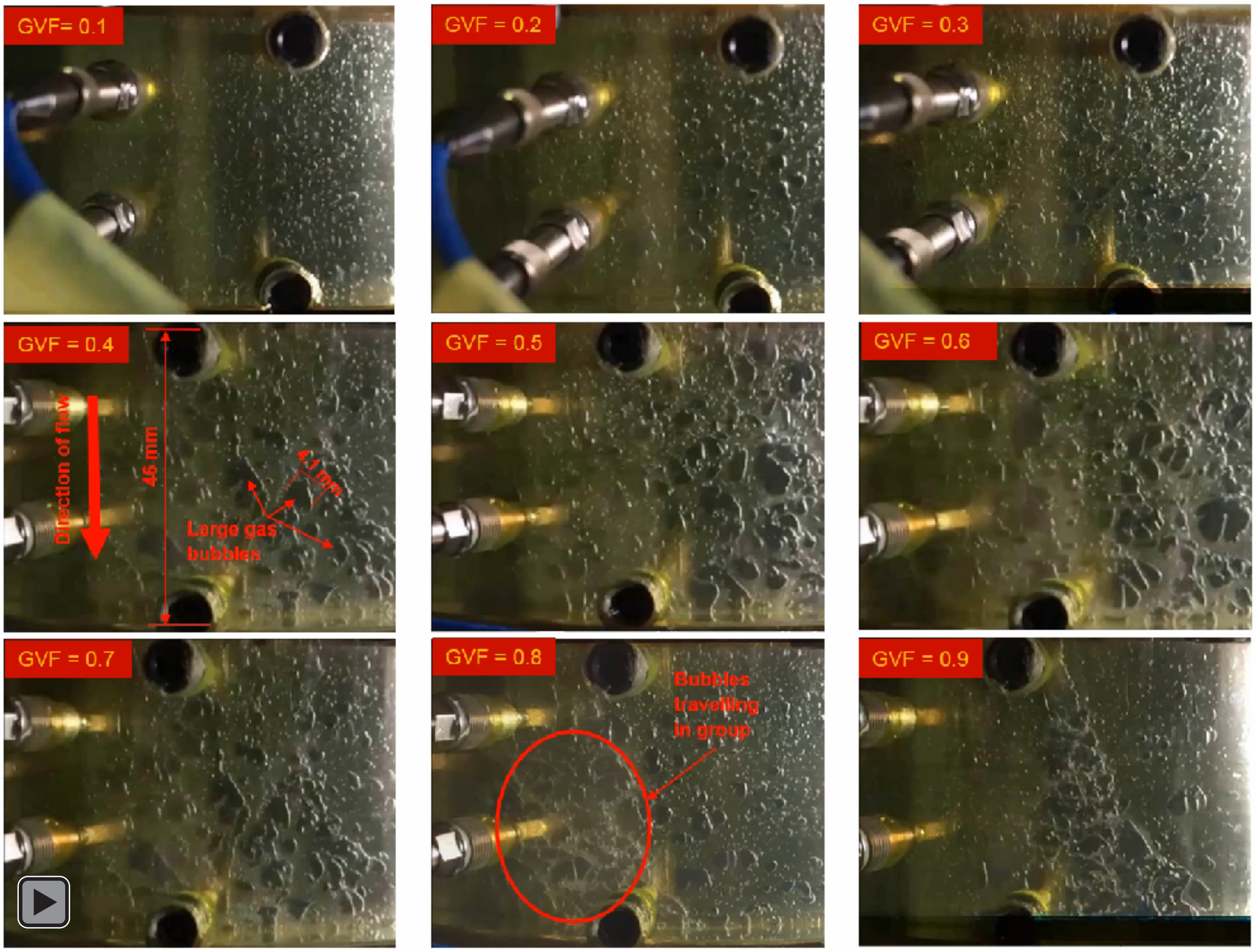

Fig. 7 Flow visualization of air-oil mixture, inlet GVF = 0-0.9 (seal #1). Supply pressure 2.5 bara, discharge pressure 1 bara. Shaft speed 0 rpm. Note *L/c* = 227. Videos at 60 frames/s taken with a stroboscope light with frequency = 30 Hz. (Click here for Web (URL) Link).

Fig. 8 Flow visualization of air-oil mixture, inlet GVF=0.9 (seal #1). Supply pressure 2 bara, discharge pressure 1 bara. Shaft speed 1.8 krpm. Videos at 60 frames/s taken with a stroboscope light with frequency = 30 Hz to freeze the shaft rotation motion. (Click here for Web (URL) Link).

COMPARISON OF LEAKAGE AMONG FIVE SEALS

The mass flow rate or leakage thru an annular seal with uniform clearance (i.e., like seal #1) is [7]

$$\dot{m}_{pl} = \left(\rho_l Q_l\right) = \frac{1}{12}\frac{\rho_l}{\mu_l}(P_s - P_a)\frac{\pi D c^3}{L} \tag{7}$$

This formula applies strictly for a laminar flow condition, largely dominated by viscous flow effects. A typical orifice-like equation to estimate the flow applies to fluid flows affected by fluid inertia (not viscous) effects. Seals with distinct geometry have a different ability to reduce leakage. Nonetheless, the mass flow is proportional to the pressure drop and much affected by the seal clearance (c).

Figure 9 shows the measured mass flow rate for each test seal operating solely with pure oil (GVF=0) and under the same pressure difference (P_s-P_a) =1.9 bar. The results are shown in dimensionless form by dividing the recorded leakage to the one of a plain seal having the same nominal clearance. As an example, for the grooved seal with c_{min}=0.211mm, the measured $\dot{m}_{pl}$ = 223 g/s; and Eq. (7) with c=0.211mm predicts a flow of 132 g/s. Hence, the dimensionless leakage is 223/132=1.69. For the three wave seal, Eq. (7) uses c=c_m=0.191 mm; whereas for the upstream/downstream step clearance seals, c=0.274 mm.

In Fig. 9, the uniform clearance seal shows a unit (dimensionless) leakage, whereas the three-wave seal leaks 20% more. The grooved seal leaks the most, and the downstream step clearance seal leaks the least. Note that for the grooved seal, the Reynolds numbers, axial and circumferential, $Re_z = \frac{\dot{m}_{pl}}{\pi D \mu_l} = 54$ and $Re_c = \frac{\rho_l \Omega R c}{\mu_l} = 392$ evidence laminar flow; that is a flow dominated by viscous forces rather than fluid inertia ones. The grooves (d_g/c_r=2.6) effectively decrease the flow resistance, hence its large leakage. Further research discloses that when the axial Reynolds number increases in a grooved seal, the leakage reduces quickly (see later Fig. 10).

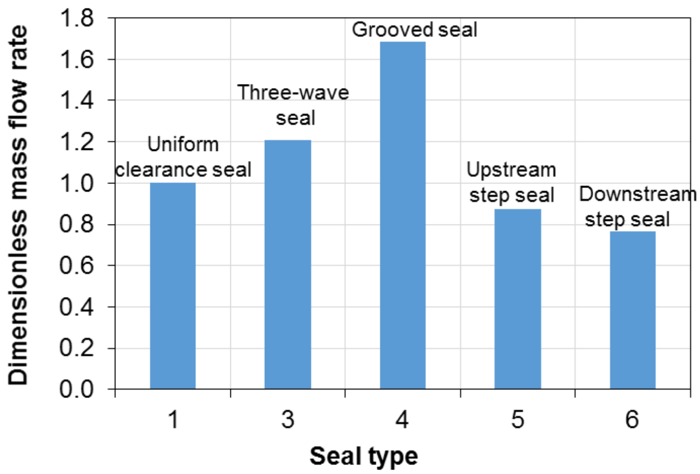

Fig. 9 Seal mass flow rate (dimensionless) for test seal types operating with liquid only.

Leakage versus inlet gas volume fraction- seals #1, #2, #3, and #4

Figure 10 shows the normalized leakage ($\bar{\dot{m}}_m$) for the uniform clearance seals (#1, #2), the three-wave seal (#3), and the grooved seal (#4) vs. inlet GVF. The leakage for each seal is normalized with respect to the flow recorded for operation with a pure liquid and a zero shaft speed condition. The solid symbols represent test data and the red lines denote predictions for the uniform clearance seals and the three-wave seal based on a BFM tool [11]. Recall the small clearance seal (#1) and the three-wave seal (#3) have a similar nominal clearance. From the tests, at a GVF=0, the three-wave seal (#3) leaks ~20% more compared with the uniform clearance seal (#1).

The normalized leakage for the first three seals is nearly the same. The test data collapses into a single representation and shows the leakage decreases steadily with an increase in inlet GVF. For uniform clearance seal #2, the one with the largest clearance, its leakage reduces slightly faster with GVF when compared with the data for the other two seals. The predictions (red line) agree with the test results, thus giving credence to the flow model. The normalized leakage for the grooved seal reduces quickly as the inlet GVF increases. Note the mixture axial Reynolds number $Re_z = \frac{\dot{m}_m}{\pi D \mu_m}$ at the seal exit plane increases from 54 for operation with pure oil (GVF=0) to 238 for operation with a mixture with inlet GVF = 0.7.

As a note of interest (Fig. 10b), for operation with pure oil or a low GVF (< 0.3), the three-wave seal shows a 35% increase in leakage as the shaft speed increases from 0 rpm to 4 krpm (ΩR = 26.7 m/s). The increase is due to thermal effects induced by shear drag when the rotor turns. The temperature rise lowers the oil viscosity, and hence the leakage raises. An increase in mixture GVF (>0.4) lowers the drag torque, see Fig. 11, and lessens the temperature rise; hence the little influence on $\dot{m}_m$ for operation with a large gas content in the mixture.

Note that the density of the mixture, ρ_m = (1-GVF)·ρ_l + GVF·ρ_g, reduces by ~20% when the inlet GVF increases from 0 to 0.2, as shown in Table 2, since $\rho_g << \rho_l$. On the other hand, the (normalized) mass flow remains approximately the same as that for the pure oil condition, thus the volumetric flow rate will increase by ~20%. At a GVF=0.8, $\dot{m}_m$ ~ 0.9, but the mixture density has decreased to 20% (ρ_m ~ 0.2 ρ_l), which lead to an increase in volumetric flow rate of ~4.5 times that of the pure liquid case. The rapid change in flow will influence the development of the circumferential velocity along the flow direction, and thus also affect the seal force coefficients.

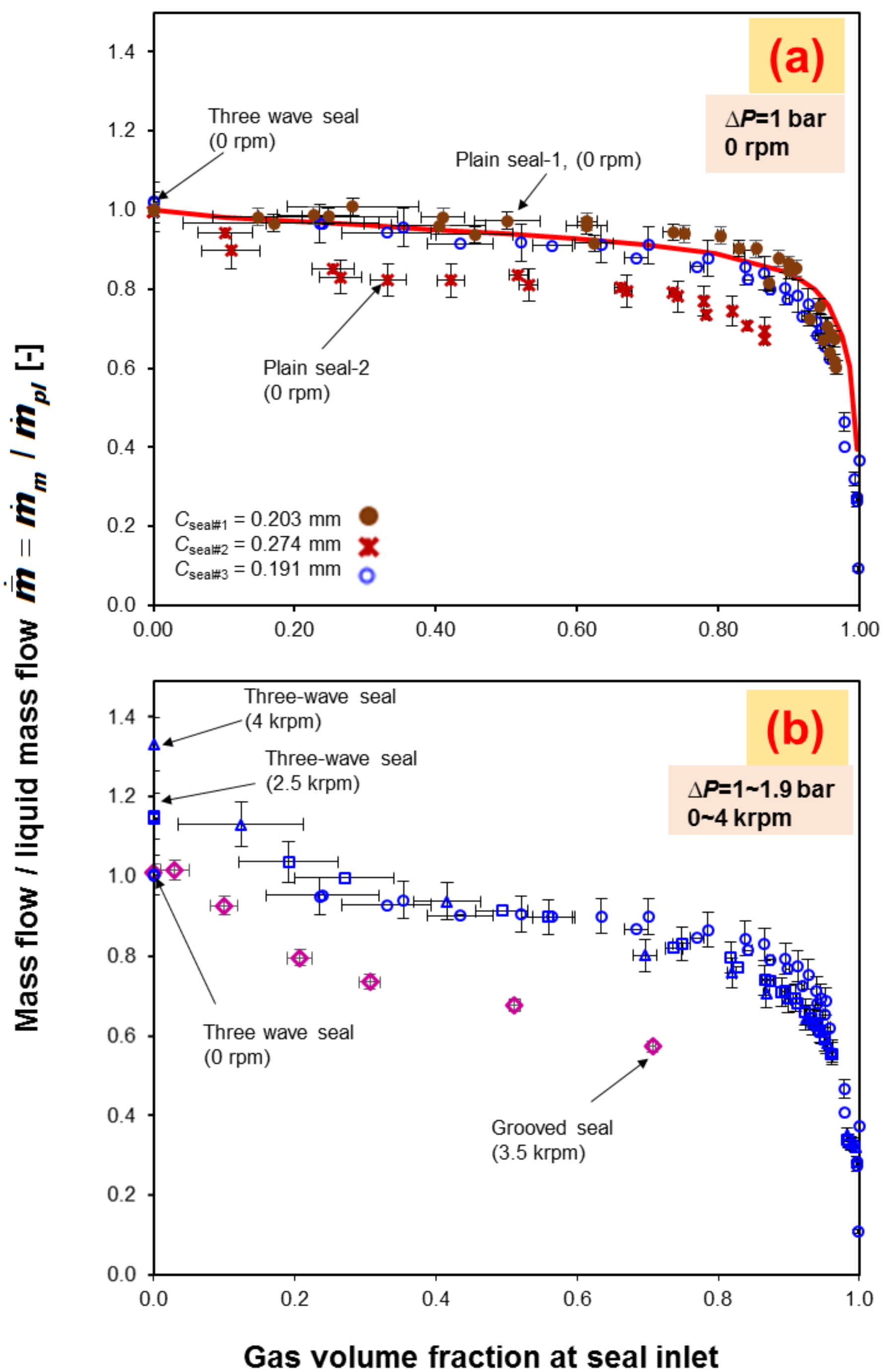

Fig. 10 Normalized leakage ($\dot{m}_m$) vs GVF for two plain (uniform clearance) seals, a three-wave clearance seal, and a grooved seal. Top (a) without shaft speed; bottom (b) with shaft speed to 4 krpm (26.6 m/s). Mass flow rate for seal with a pure oil ($\dot{m}_{pl}$): plain seal 1: uniform c_1=0.203 mm, 40 g/s (ΔP=1 bar, N=0 rpm, T_{in}=32 °C); plain seal-2: uniform c_2=0.274 mm, 149 g/s (ΔP =1 bar, N=0 krpm, T_{in}=40 °C) ; three-wave seal: c_m=0.191 mm, 53 g/s (ΔP =1 bar, N=0 rpm, T_{in}=39°C); grooved seal: c_r=0.191 mm, 223 g/s (ΔP =1.9 bar, N=3.5 krpm, T_{in}=37°C)

Table 2. Density of air-oil mixture versus GVF

ρ_l = 830 kg/m^3, ρ_g=2.9 kg/m^3 at 2.5 bara and 20 °C.

GVF	0	0.1	0.2	…	0.8	0.9	1
Density (ρ_m)	830	747	665	…	168	86	2.9
ρ_m / ρ_l	1	0.900	0.801		0.203	0.103	0.003

Drag torque versus inlet gas volume fraction for plain seal #1

Seals having small drag power losses contribute to the efficiency of a turbomachinery. Hence, recording the drag torque is of importance; in particular in a subsea application whose flow changes composition, say from all liquid to a mixture with large gas content. A sudden increase in gas content, in an otherwise liquid stream, would produce an immediate drop in drag torque which could cause a rapid over speed or tripping of the rotating machinery. Unless quickly controlled or contained, the integrity of the rotating machinery would be compromised.

Figure 11 shows the experimentally estimated (symbols) and predicted (line) normalized drag torque $\overline{T} = T_m / T_{pl}$ for the uniform clearance seal (#1) versus inlet GVF. T_m is the drag torque for operation with a mixture, and T_{pl} is the drag torque for the seal lubricated with pure oil (GVF=0). See Ref. [19] for details on the predictive formula. In brief, the test data and predictions match. The drag torque linearly decreases as the gas content increases; hence, making rather cursory the integration of this information in a process control of the machine.

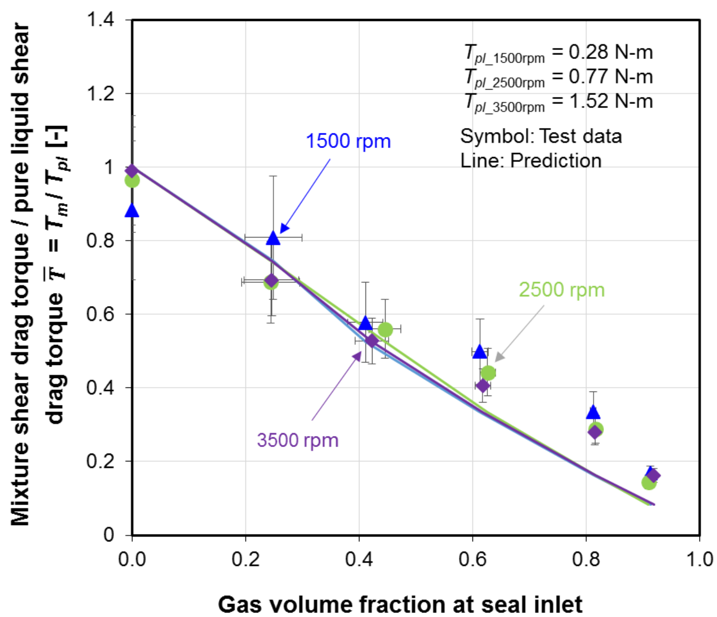

Fig. 11 Normalized seal drag torque ($\overline{T}$) vs inlet GVF for uniform clearance seal (#1).

THE PROCEDURE FOR IDENTIFICATION OF FORCE COEFFICIENTS

The identification of seal force coefficients requires first to find the test rig structure parameters in a dry (non-lubricated) condition and without shaft speed. The test rig has a structure stiffness K_S = 3.2 MN/m, mass M_S = 14.5 kg, and damping coefficient C_S = 0.38 kN s/m. Thus the system natural frequency ω_n = 78 Hz and damping ratio ζ = 3%. An impact test on the rig structure produces a natural frequency of 78.5 Hz.

While an air in oil mixture lubricates the test seal, the motor is turned on to rotate the shaft at a constant speed of (say) 3.5 krpm ($R\Omega$ = 23.3 m/s). During the dynamic load tests, one electromagnetic shaker along the X direction (see Fig. 4 for reference of coordinate) excites the seal housing with unidirectional periodic load $\mathbf{F_X} = [f_X = f_o\, e^{i\omega t}, f_Y = 0]^T$ to produce dynamic motion $\mathbf{z_X} = [X_X, Y_X]^T$ and acceleration $\mathbf{a_X} = [a_{XX}, a_{YX}]^T$, simultaneously, a data acquisition system record the time domain data for 10 seconds at 12,800 samples/s. Above, $i = \sqrt{-1}$, $\mathbf{z_X}$ is the relative displacement between the rotor and the seal housing, and $\mathbf{a_X}$ is the absolute acceleration of the seal housing. The amplitude of seal housing motion (e) is approximately 5% of the seal radial clearance. After the X-shaker stops, the Y-shaker repeats the excitation $\mathbf{F_Y} = [f_X = 0, f_Y = f_o\, e^{i\omega t}]^T$ to produce the motion $\mathbf{z_Y} = [X_Y, Y_Y]^T$ and acceleration $\mathbf{a_Y} = [a_{XY}, a_{YY}]^T$.

San Andrés [20] details a parameter identification procedure for in the frequency domain. First, a Discrete Fourier Transformation method transfers the recorded time domain data into the frequency domain, i.e., $\mathbf{F}_{\mathbf{X}(\omega)}$ = DFT($\mathbf{F}_{\mathbf{X}(t)}$). Define the (2x2) matrices in the frequency domain: force $\mathbf{F}_{(\omega)} = [\mathbf{F}_{\mathbf{X}(\omega)} \mid \mathbf{F}_{\mathbf{Y}(\omega)}]$, seal housing acceleration $\mathbf{A}_{(\omega)} = [\mathbf{A}_{\mathbf{X}(\omega)} \mid \mathbf{A}_{\mathbf{Y}(\omega)}]$, and seal to rotor relative displacements $\mathbf{Z}_{(\omega)} = [\mathbf{Z}_{\mathbf{X}(\omega)} \mid \mathbf{Z}_{\mathbf{Y}(\omega)}]$. The test system has a complex stiffness matrix (**H**) determined from

$$\mathbf{H}_{(\omega)} = [\mathbf{F}_{(\omega)} - M_S \mathbf{A}_{(\omega)}]\, \mathbf{Z}_{(\omega)}^{-1} \tag{8}$$

Subtracting the structure force coefficients from the system **H** yields the seal dynamic complex stiffness

$$\mathbf{H}_{\mathrm{Seal}} = \mathbf{H} - [\mathbf{K}_s + i\omega \mathbf{C}_s] \tag{9}$$

In a liquid seal, the complex stiffness can be defined in terms of constant parameters (stiffness, viscous damping and added mass) as

$$\mathbf{H}_{\mathrm{Seal}(\omega)} = [\mathbf{K} - \omega^2 \mathbf{M} + i\omega \mathbf{C}]_{\mathrm{Seal}} \tag{10}$$

In a *wet* seal, the mixture is compressible due to the gas content; and the force coefficients are frequency dependent. Rewrite $[\mathbf{H}]_{\mathrm{Seal}(\omega)}$ as

$$\mathbf{H}_{\mathbf{seal}(\omega)} = \mathbf{H}(\omega)^{\parallel} + i\, \mathbf{H}(\omega)^{\perp} \tag{11}$$

where $\mathbf{H}^{\parallel}$ is the dynamic complex stiffness that is in parallel with the displacement vector **Z**, and $\mathbf{H}^{\perp} = \omega \boldsymbol{C}$ is the quadrature stiffness, perpendicular to the displacement or parallel to the velocity vector $\dot{\mathbf{Z}}$. Seals that operate in a centered condition show $H_{XX} = H_{YY}$ and $H_{XY} = -H_{YX}$, thus for simplicity the following sections present the seal complex stiffnesses as $H_D^{\parallel} = \frac{H_{XX}^{\parallel} + H_{YY}^{\parallel}}{2}$ and $H_C^{\parallel} = \frac{H_{XY}^{\parallel} - H_{YX}^{\parallel}}{2}$, etc.

FORCE COEFFICIENTS FOR TWO PLAIN SEALS AND A THREE-WAVE SEAL

Figures 12 to 14 depict the components of the dynamic stiffness ($\mathbf{H}_{\mathrm{Seal}}$) versus frequency ($\omega$) for the two plain annular seals (#1 and 2) and the three-wave seal (#3). The specific operating conditions are inlet pressure P_s = 2.5 bara, inlet GVF = 0 to 0.9, and shaft speed = 3.5 krpm (ΩR = 23.3 m/s). The symbols show test data whereas lines denote the BFM predictions, a solid line for the three-wave seal (#3) and a dashed line for plain seal #1. Vertical error bars denote the variability of test data along the *X* and *Y* directions. Ref. [21] details in full the comparisons to reveal the advantages of the wavy-seal and its degradation as its unique clearance wears out.

Figure 12 shows the direct dynamic stiffnesses ($H_D^{\parallel}$) versus frequency (ω). The various graphs depict $H_D^{\parallel}$ for four inlet GVFs=0 (liquid), 0.2, 0.6 and 0.9. Amongst the three seals, the wavy seal (#3) shows a larger dynamic stiffness than seal #1, mainly on account of its mechanical preload. A worn seal (#2), the one with the largest clearance, shows a negligible static stiffness at $\omega \rightarrow 0$. For operation with a pure liquid (GVF=0), $H_D^{\parallel}$ for both plain (uniform clearance) seals and the three-wave seal decreases with frequency (ω^2), as the liquid seals generate a large added mass (M) effect, $H_D^{\parallel} \rightarrow (K-\omega^2 M)$. For operation with a mixture (GVF increases), the magnitude of $H_D^{\parallel}$ generally follows as: three-wave seal > plain seal #1 > plain seal #2. $H_D^{\parallel}$ increases (hardens) with frequency (ω) for the seals having a relatively small clearance (#1). Note the three-wave seal shows a remarkable "stiffening" effect as $H_D^{\parallel}$ >0 for operation with GVF as large as 90%. That is, operation with a gas content makes the seal *hard* to push and will affect the rotor-bearing system critical speeds.

Figure 13 shows the cross-coupled dynamic stiffness ($H_C^{\parallel}$) versus frequency (ω) for the three test seals. The wavy seal (#3) produces the largest cross coupled stiffness, followed by the plain seal #1, and next by the worn seal (#2). For the three seals lubricated with a pure liquid (GVF = 0), $H_C^{\parallel}$ is frequency independent. However, a mixture whose inlet GVF = 0.2→0.9 produces frequency dependent $H_C^{\parallel}$. Surprisingly, for operation with a mixture, the three seals show the smallest cross-coupled dynamic stiffness ($H_C^{\parallel}$) at a frequency near the shaft running speed (58 Hz=1X). No rationale is known for this peculiar outcome.

The test data shows the quadrature stiffness $H^{\perp}$is proportional to the excitation frequency (ω); hence not shown for brevity. Importantly, the results evidence constant damping coefficients over the excitation frequency range. Figure 14 shows the direct damping coefficient ($C = H^{\perp}/\omega$) versus inlet GVF for the three seals. The three-wave seal (#3) shows ~50% more damping compared with that of the uniform clearance seal #1; the large clearance plain seal (#2) shows the smallest magnitude. Not surprisingly, the damping coefficient (C) decreases continuously as the mixture inlet GVF increases from 0 to 0.9. However, the large clearance seal (#2) shows a constant damping for operation with a mixture with inlet GVF up to 0.2.

The predicted $H_D^{\parallel}$ and $H_C^{\parallel}$ for seals #1 and #3 (wavy) match the respective test result for operation with a pure liquid. For operation with a mixture with GVF≤0.2, the BFM produces results similar in magnitude to the test data only at a low frequency. The BFM over predicts $H_D^{\parallel}$ and under predicts $H_C^{\parallel}$ at high frequency. For operation with large GVFs, the BFM under predicts both $H_D^{\parallel}$ and $H_C^{\parallel}$ for any frequency. Unlike the test data for damping reported in Fig.14, the BFM produces frequency dependent damping coefficients for operation with a mixture. The predictions are thus poor and not shown.

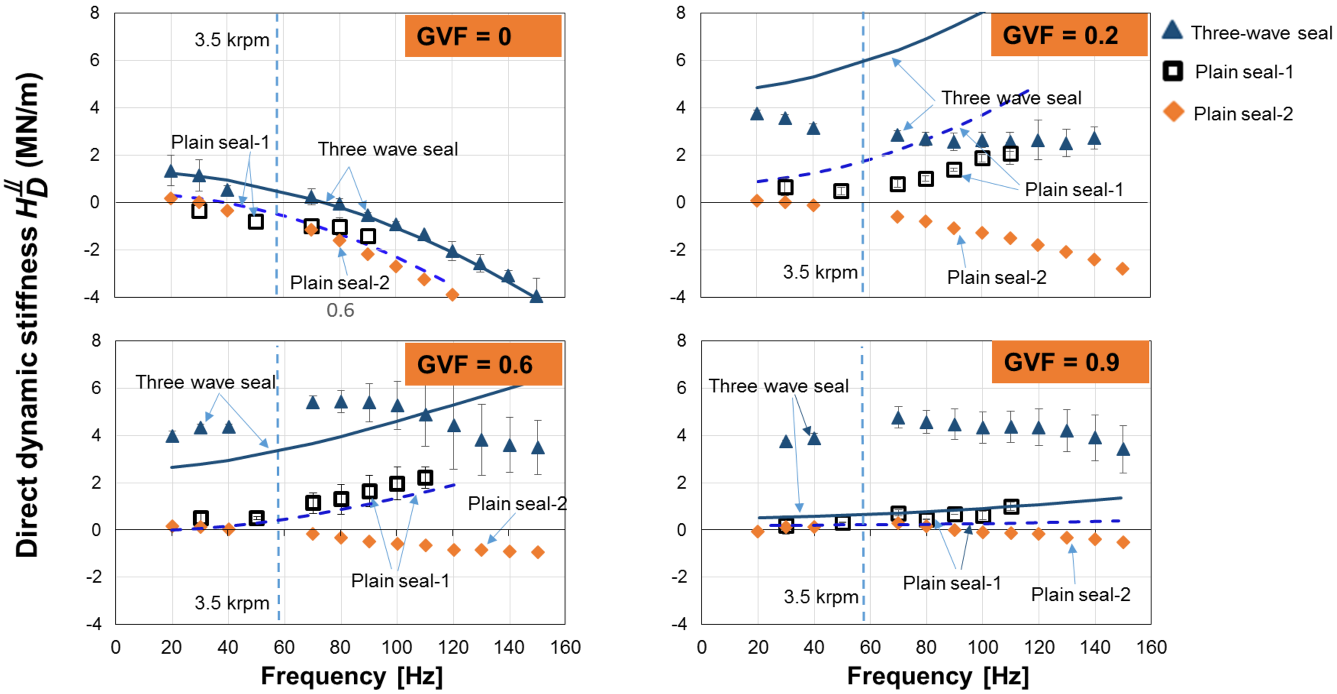

Fig. 12 Direct dynamic stiffness versus frequency: two plain (uniform clearance) seals and a three-wave seal. Inlet GVF = 0 to 0.9. Shaft speed = 3.5 krpm (ΩR = 23.3 m/s). Supply pressure (P_s) = 2.5 bara, discharge pressure (P_a) = 1 bara. Lines: prediction; Symbols: test data.

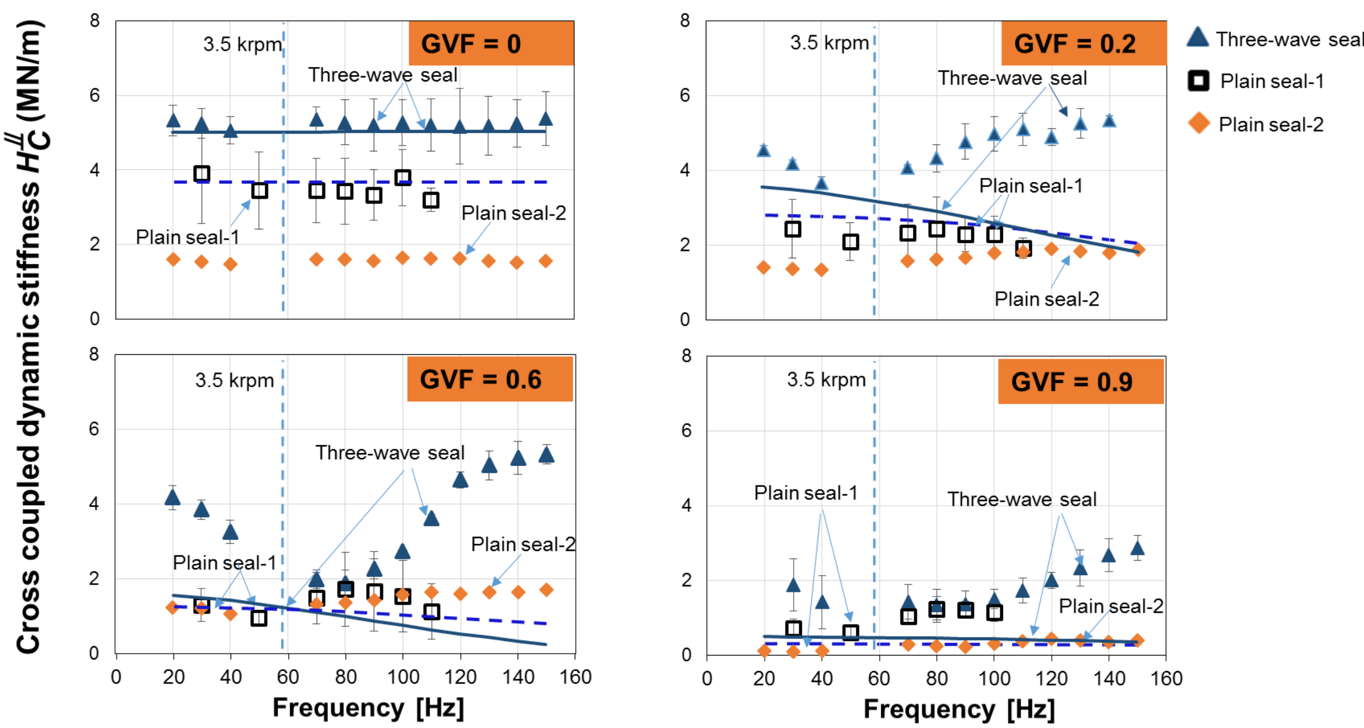

Fig. 13 Cross coupled dynamic stiffness versus frequency: two plain (uniform clearance) seals and a three-wave seal. Inlet GVF = 0 to 0.9. Shaft speed = 3.5 krpm (ΩR = 23.3 m/s). Supply pressure (P_s) = 2.5 bara, discharge pressure (P_a) = 1 bara. Lines: prediction; Symbols: test data.

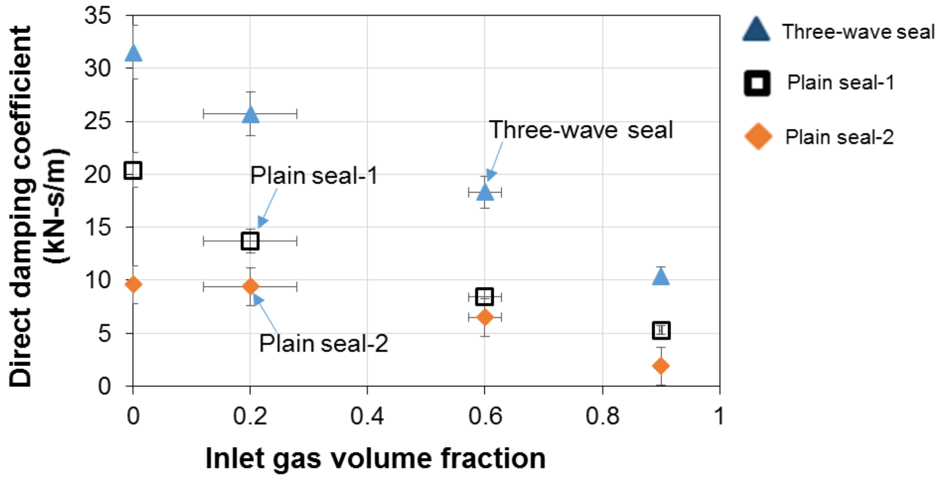

Fig. 14 Direct damping (C_{Seal}) coefficient versus inlet GVF: two plain (uniform clearance) seals and a three-wave seal. Inlet GVF = 0 to 0.9. Shaft speed = 3.5 krpm (ΩR = 23.3 m/s). Supply pressure (P_s) = 2.5 bara, discharge pressure (P_a) = 1 bara.

Figure 15 shows the effective damping coefficient ($C_{eff} = C - k/\omega$) vs. frequency (ω) for the three seals. The graphs show results for GVF=0, 0.2, 0.6 and 0.9. Test data is in symbols and lines denote BFM predictions. A positive C_{eff} is best as it dissipates mechanical energy from rotor whirl motions. The three-wave seal shows the greatest C_{eff} at $\omega > \omega_c$, where ω_c is the cross-over frequency. For operation with mainly oil (GVF $\leq$ 0.4), C_{eff} increases with frequency for the three seals. However, for the wavy seal operating with a mixture with GVF > 0.4, C_{eff} first increases with frequency until ω reaches 1X, C_{eff} then decreases as the frequency increases further. For the three seals, C_{eff} drops quickly in magnitude with an increase in mixture GVF. The BFM predicts well C_{eff} for both seals #1 and #3 for operation with a mainly oil condition (GVF≤0.2). For operation with a large gas content (GVF≥0.6), the BFM largely under predicts C_{eff}. In brief, the experimental C_{eff} is larger than the overly conservative prediction.

Incidentally, the test results and predictions show a whirl frequency ratio $WFR = k/(\Omega\ C) \sim 0.5$ for operation with either pure oil or a mixture with small to moderate GVF (<0.6). In the graphs this result is denoted by the cross-over frequency at which C_{eff} turns positive, shown as ½ X. The result is expected since the flow regime is laminar.

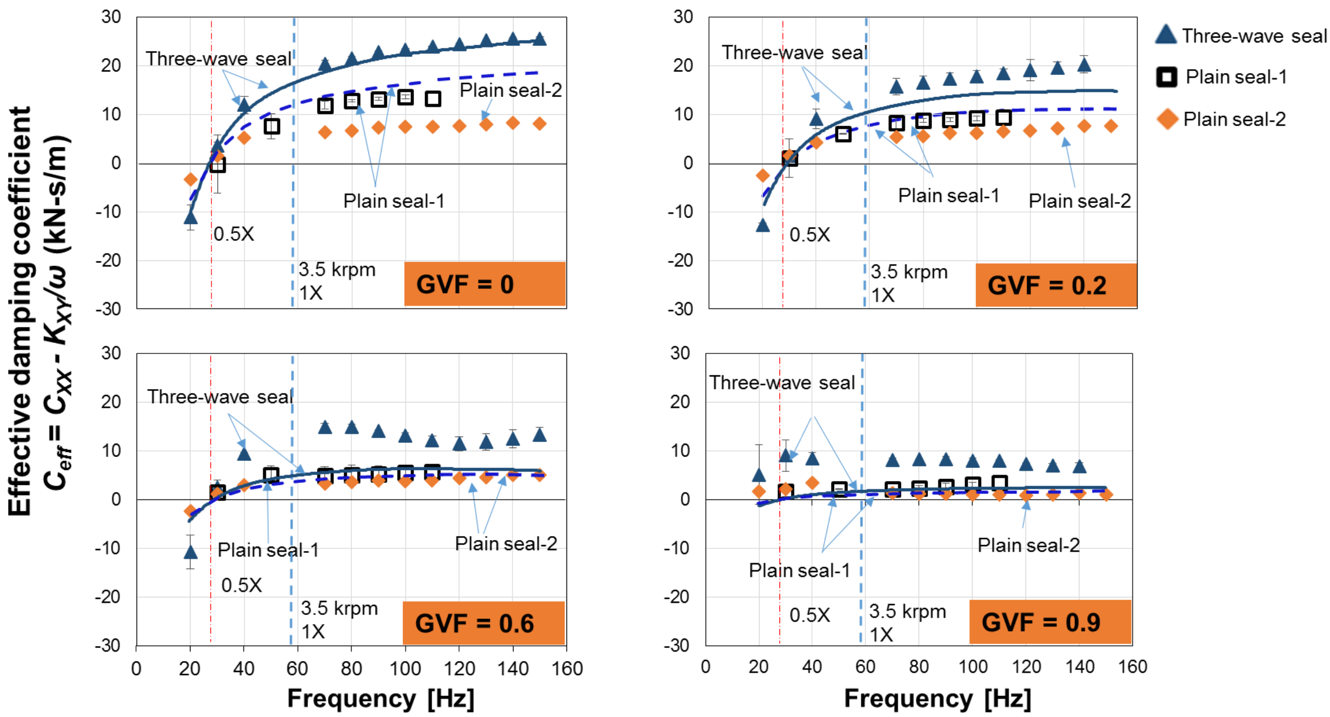

Fig. 15 Effective damping coefficient ($C_{eff} = C - k/\omega$) **vs. frequency: two plain (uniform clearance) seals and a three-wave seal.** Inlet GVF = 0 to 0.9. Shaft speed = 3.5 krpm (ΩR = 23.3 m/s). Supply pressure (P_s) = 2.5 bara, discharge pressure (P_a) = 1 bara. Lines: prediction; Symbols: test data.

FORCE COEFFICIENTS FOR A GROOVED SEAL

Grooved seals are commonly used as wear ring seals [22] and balance drum pistons [23] in pumps. A grooved seal has less leakage compared with a uniform clearance seal if the flow condition is turbulent; not so for laminar flow. In addition, these seals also show a distinct forced performance when operating with a gas-liquid two component flow. Note there is no predictive model to correlate the test results shown below. Recall the test grooved seal has a radial clearance $c = 0.211$ mm, groove depth $d_g = 0.543$ mm (d_g/c= 2.6) and length $l_g = 1.5$ mm (l_g/L=0.035), and groove land length $l_l = 0.904$ mm (l_l/L=0.02). The number of grooves N_g= 14.

Figure 16 shows the direct dynamic stiffness ($H_D^{//}$) versus frequency for operation with inlet GVF varying from 0 (pure oil) to 0.7 (mostly gas). The supply pressure P_s=2.9 bara and the shaft spins at 3.5 krpm ($R\Omega$ = 23.3 m/s). For operation with a mainly oil case (GVF $\leq$ 0.1), $H_D^{//}$ shows a quadratic reduction with frequency (ω); hence $H_D^{//} \rightarrow (K - M\omega^2)$ delivers a static stiffness K= 0.3 MN/m and inertia M=6.7 kg. A small gas content (GVF = 0.1) does not change the direct stiffness but reduces the added mass coefficient to 5.3 kg. For operation with a mixture with GVF = 0.2→0.7, $H_D^{//}$ ~0, i.e., it reduces to a negligible magnitude. The behavior contrasts with that of the *hardening* stiffness in seals #1 and #2 with a uniform clearance or the three-wave seal (#3) shown in Figure 12 (GVF=0.2, 0.6 and 0.9). In brief, the groove seal lacks stiffness when operating with a gas in oil mixture with GVF>0.2.

Figure 17 shows the cross coupled dynamic stiffness ($H_C^{//}$) versus frequency. Operating at a shaft speed 3.5 krpm, $H_C^{//}$ is larger than the direct stiffness. When lubricated with a pure oil, the grooved seal shows frequency independent cross coupled dynamic stiffness. When the inlet GVF increases from 0.1 to 0.7, $H_C^{//}$ increases with frequency, but reduces with inlet GVF. For operation with a pure liquid, the grooved seal (#4) produces ~1/5 $H_C^{//}$ compared with the three wave seal (#3), and 1/3 $H_C^{//}$ compared with seal #1. As with the other seals, the quadrature dynamic stiffness is proportional to excitation frequency; hence the direct damping coefficient (C) is constant over the excitation frequency range (20 Hz-150 Hz). Figure 18 depicts $C = (H^{\perp}/\omega)$ decreasing steadily with GVF > 0.20. A large inlet GVF =0.7 reduces the direct damping by ~ 55% compared to the pure oil (GVF=0) condition. In general, the grooved seal show a similar damping magnitude as the large clearance seal (#2).

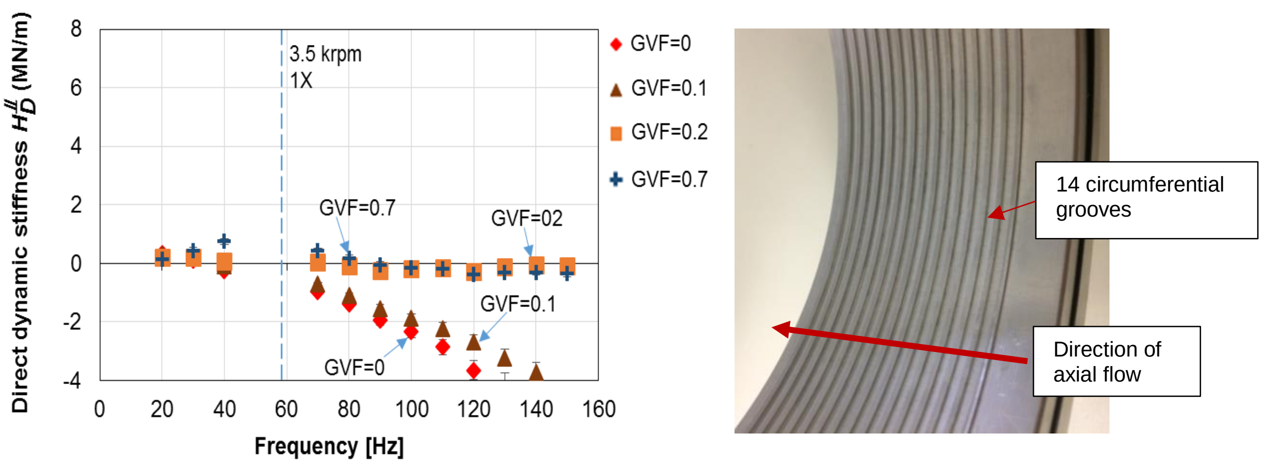

Fig. 16 Grooved seal: direct dynamic stiffness versus frequency. Inlet GVF = 0, 0.1, 0.2 and 0.7. Shaft speed = 3.5 krpm (ΩR = 23.3 m/s). Supply pressure (P_s) = 2.9 bara, discharge pressure (P_a) = 1 bara.

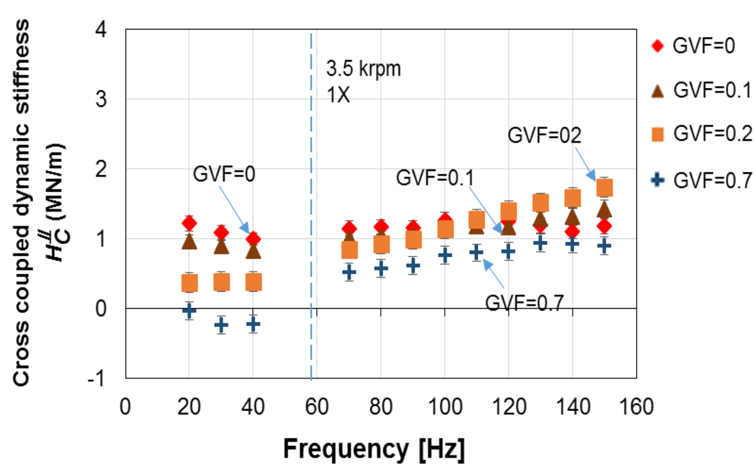

Fig. 17 Grooved seal: cross coupled dynamic stiffness versus frequency. Inlet GVF = 0, 0.1, 0.2, 0.7. Shaft speed = 3.5 krpm (ΩR = 23.3 m/s). Supply pressure (P_s) = 2.9 bara, discharge pressure (P_a) = 1 bara.

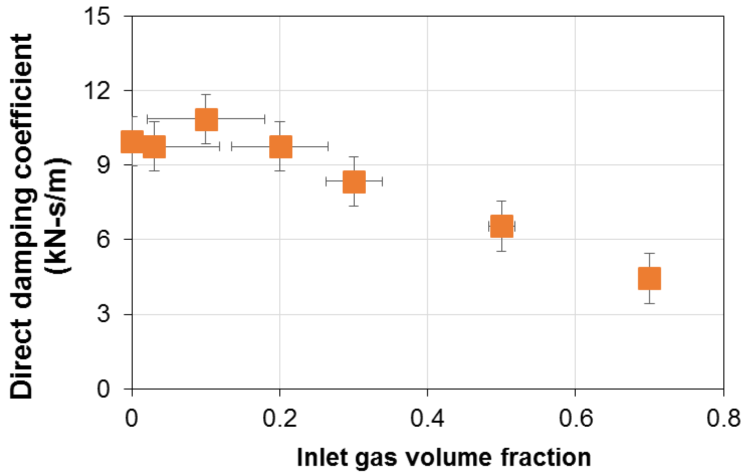

Fig. 18 Grooved seal: direct damping coefficient versus inlet gas volume fraction. Shaft speed = 3.5 krpm (ΩR = 23.3 m/s). Supply pressure (P_s) = 2.9 bara, discharge pressure (P_a) = 1 bara. Coefficient valid for frequency range 20 Hz-150 Hz.

Figure 19 shows the groove seal effective damping (C_{eff}) versus frequency and various GVFs. The only liquid seal shows C_{eff} increasing with frequency. If lubricated with a low GVF (0.1, 0.2) C_{eff} is remarkably greater (than for the pure liquid) because the direct damping (C) remains constant. Even though the circumferential grooves reduce the cross coupled stiffness, compared with that of the uniform clearance seal (see Fig, 13), the direct damping coefficient also reduces, thus C_{eff} for the groove seal (#4) is lower than the uniform clearance seal (#1) and the three-wave seal (#3). The grooved seal shows a smaller cross frequency (~0.33) compared with the rest seals (#1 to #3).

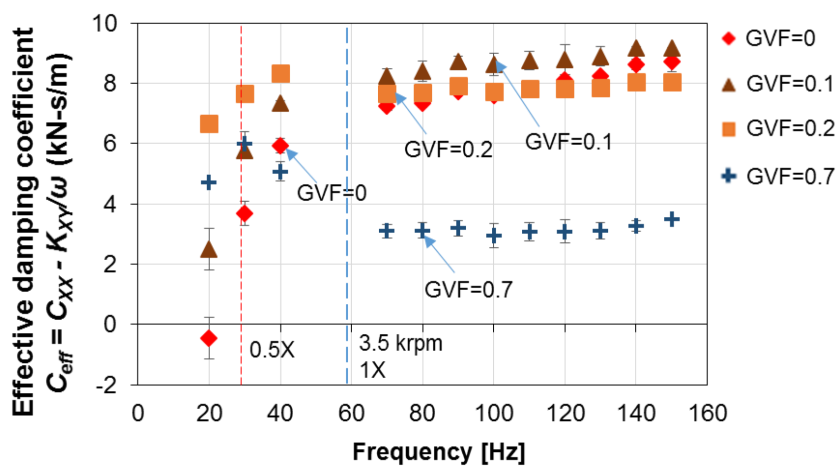

Fig. 19 Grooved seal: effective damping coefficient vs. frequency. Inlet GVF = 0 to 0.7. Shaft speed = 3.5 krpm (ΩR = 23.3 m/s). Supply pressure (P_s) = 2.9 bara, discharge pressure (P_a) = 1 bara.

FORCE COEFFICIENTS FOR STEPPED CLEARANCE SEALS

Pumps and hydraulic turbines often use (upstream) step clearance seals with a narrow clearance facing the incoming external flow. These seals are known to cause spontaneous (self-excited) shaft vibrations, even without rotor spinning. However, when implementing a downstream step clearance seal (reverse orientation), the same machine does not suffer a similar mishap [24]. There is no test data asserting to the cause of this phenomenon.

This section presents the (direct) dynamic force coefficients of two types of stepped clearance seals, both having the same axial length L=43.4 mm and diameter D=127 mm (L/D=0.34). The upstream step clearance seal (#5, USCS) begins with a narrow clearance c_T=0.174 mm over length L_T = 4.6 mm, and ends with a large clearance c_B = 0.274 mm over a wide length L_B = 38.8 mm; c_B/c_T = 1.57 and L_B/L_T = 8.43. The downstream step clearance seal (#6, DSCS) starts with a large clearance c_T = 0.274 mm over a wide length L_T = 35.4 mm, and followed by a narrow clearance c_B = 0.174 mm over as short span of length L_B = 8 mm; c_T/c_B = 1.57 and L_T/L_B = 4.42.

Both seals are lubricated with ISO VG 10 oil supplied at 30°C. During the tests, the shaft speed increases discretely from 0 to 3.5 krpm (ΩR=23.3 m/s) and the supply pressure varies from 1.8 bara to 3.5 bara. While in operation, impact loads, along the X and Y axes, are exerted on the seal housing. The recorded forces and ensuing housing motions allow the identification of force coefficients.

Operation with liquid (oil) only

The following data pertains to operation with pure oil only. Figure 20 depicts the direct dynamic stiffness ($H_D^{/\!/}$) versus frequency for both the upstream step clearance seal (left) and the downstream step clearance seal (right) for operation with an increasing supply pressure (P_S) and a stationary shaft. The test data estimated from a spinning shaft is similar to that obtained from the zero speed condition, thus not shown for simplicity. Do note test data with shaft rotation (and cross-coupled stiffness) is shown in Fig. 21.

For the upstream step clearance seal, $H_D^{/\!/} < 0$ for $\omega \to 0$[4], which produces a negative static stiffness (K)! As the pressure increases from 1.8 to 2.9 bara, $H_D^{/\!/}$ shifts to a lower magnitude with a similar curvature, indicating that the increase in flow rate increases the magnitude of the negative static stiffness but not the added mass (M) since $H_D^{/\!/} \sim (K\text{-}\omega^2 M)$. On the other hand, for the other seal with the lubricant flowing first through a large clearance (c_T = 0.274 mm) and exit the seal after crossing a small clearance (c_B = 0.174 mm), akin to a converging clearance along the flow direction, $H_D^{/\!/} > 0$ as $\omega \to 0$, for operation with various P_s. Hence, the downstream step clearance seal shows a positive static stiffness (K>0). In addition, an increase in flow rate (P_s) causes $H_D^{/\!/}$ to shift to a greater magnitude, thus promoting the generation of K.

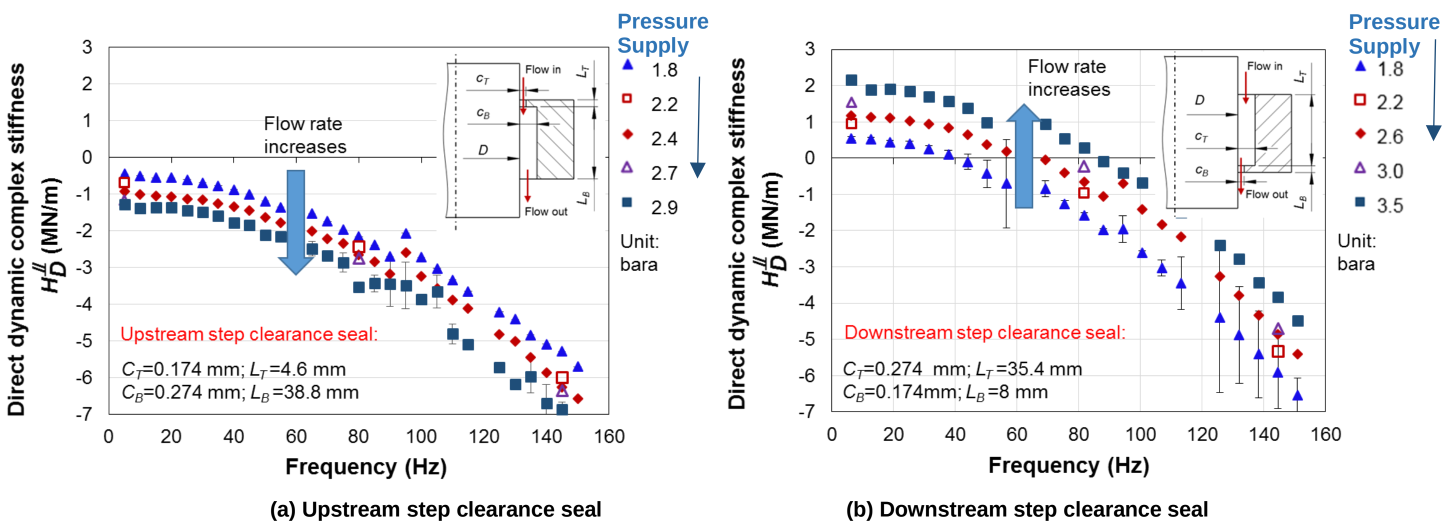

Fig. 20 Direct dynamic stiffness versus frequency for two step clearance seals. Oil supply pressure (P_s) =1.8 bara to 3.5 bara, discharge pressure (P_a) = 1 bara. Shaft speed = 0 rpm.

For both step clearance seals, Figures 21 depicts the measured and predicted direct and cross coupled stiffness coefficients (K, k) versus oil supply pressure. The test data was obtained with shaft speed equal to 1 krpm and 3.5 krpm. The predictions are derived from a (yet to be published[5]) simple model for a laminar flow step clearance seal. The experimental K and M coefficients are identified from a least square fit of $H_D^{/\!/} \to K - \omega^2 M$., whereas the cross coupled stiffness (k) derives from $H_C^{/\!/} \to k - \omega^2 m$ with m=0 for convenience.

For the upstream step clearance seal, both prediction and test data show $K < 0$, its magnitude increasing with P_s. For the downstream step clearance seal, $K > 0$ and increasing linearly with P_s. Compared with the plain seal #3 with the same large clearance (0.274 mm), see Fig. 12, the upstream step clearance seal is much softer (K<0), whereas the downstream step clearance seal is much stiffer. For example, for operation with P_s= 2.5 bara, plain seal #3 shows a static stiffness K=0.25 MN/m, whereas the downstream step clearance seal has K=1.16 MN/m, nearly five times fold! For both seals, note the predictions deliver K=0 when P_s=P_a, i.e. without any liquid flowing through the seal.

As depicted in Fig. 21b, the cross coupled stiffness (k) increases almost linearly with shaft speed. Figure 22 depicts the direct damping and mass coefficients (C, M) vs. supply pressure (P_s) for both seals lubricated with pure oil. As noted in Fig. 22b, C ~ 19.5 kN·s/m for both seals, nearly independent of P_s. The predicted C is ~20% lower than the test magnitude. Note also the seal whirl frequency ratio, WFR=$k/C\,\omega$, equals 0.5, see Table 3.

An increase in pressure from 1.8 bara to 3.5 bara affects little the inertia coefficient (M) for both seals. The predictions under predict M by 15% for the downstream step clearance seal. Note in both Figs. (21) and (22), an increases in shaft speed does not affect the direct stiffness (K) or the added mass (M) coefficients. Only the direct damping (C) reduces slightly at a speed of 3.5 krpm because the shaft speed causes a rise in fluid temperature due to the viscous shear effect. The fluid viscosity then falls down, causing a reduction in the

4 Zero frequency excitation is akin to a static displacement of the rotor within its seal.
5 The prediction is from an analytical solution obtained for a finite length step clearance seal. The model will be detailed in an upcoming paper.

damping coefficient.

Importantly enough, both damping (C) and added mass (M) coefficients do not vary significantly with the supplied flow rate (or the supply pressure P_s). The direct stiffness K does! As reported in the literature, the narrow-wide step clearance seal (USCS) is statically unstable since $K < 0$!

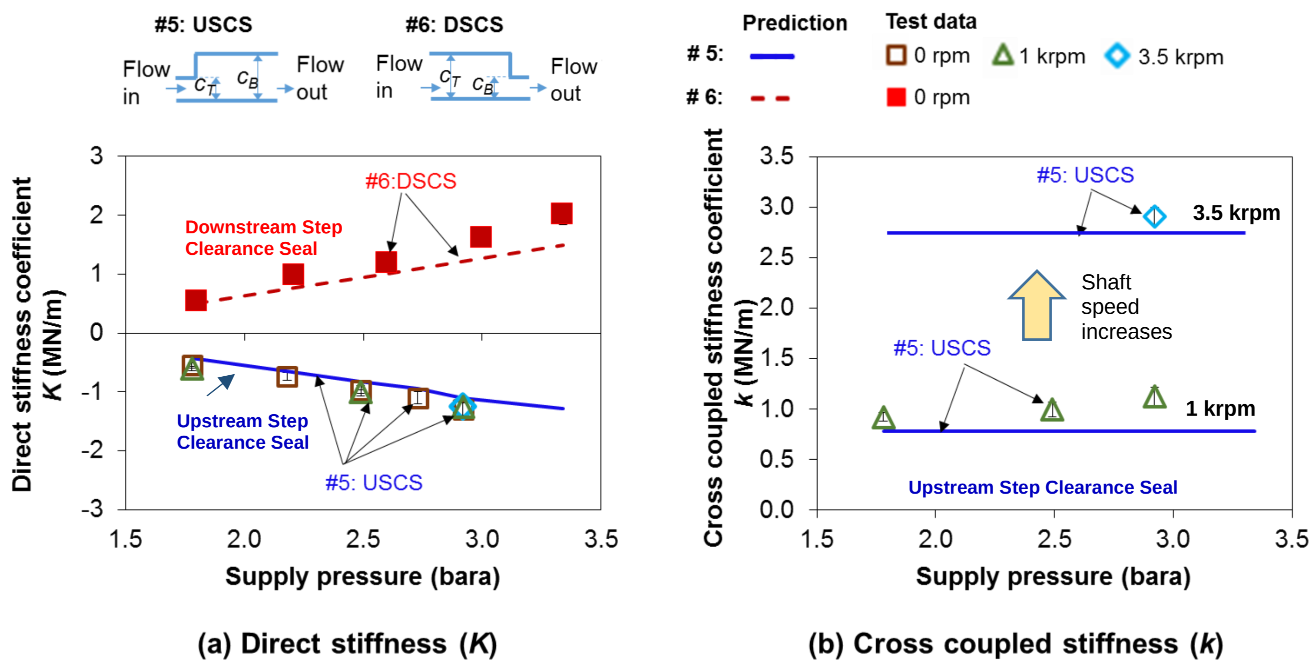

Fig. 21 Step clearance seals: Direct stiffness (*K*) and cross coupled stiffness (*k*) vs. supply pressure. Upstream and downstream step clearance seals. All liquid. Shaft speed 0, 1 krpm, and 3.5 krpm (ΩR=23.3 m/s). Lines: prediction; Symbols: test data.

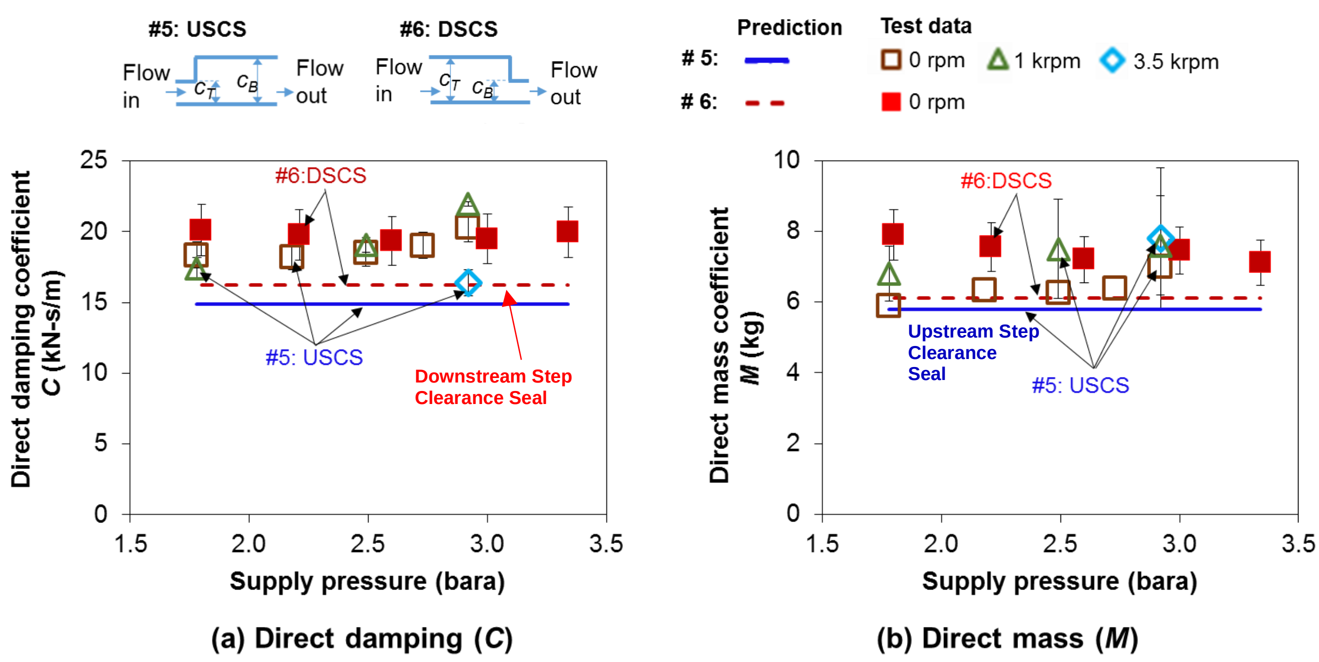

Fig. 22 Step clearance seals: Direct damping (*C*) and mass coefficients (*M*) vs. supply pressure. Upstream and downstream step clearance seals. All liquid. Shaft speed 0, 1 krpm, and 3.5 krpm (ΩR=23.3 m/s). Lines: prediction; Symbols: test data.

Operation with a gas in liquid mixture

Figure 23 depicts the direct dynamic stiffness ($H_D^{//}$) of the upstream step clearance seal (#5: USCS) lubricated with an air in oil mixture. In the test, the shaft is 1,000 rpm (16.7 Hz). The oil flow rate is constant while the air flow increases discretely to make a mixture with inlet GVF = 0.1 to 0.6. An increase in inlet GVF does not have significant effect on the direct dynamic stiffness at a low frequency, say, 10 Hz. However, air injection with inlet GVF = 0.2 reduces the drop of ($H_D^{//}$) with frequency; that is, the seal direct dynamic stiffness becomes less negative compared to that for a pure oil condition (GVF=0). The gas content in the mixture makes the fluid compressible and reduces the added mass ($M \rightarrow 0$) as the excitation frequency increases. Pump designers should be aware of the change in direct dynamic stiffness ($H_D^{//}$) to better predict rotordynamic performance.

Hence, the test results validate the *old* engineering practice that calls for air injection in the neck-ring seal of a hydraulic turbine to stabilize it [26]. In the test results, a further increase of inlet GVF to 0.6 does not appear to affect any longer the direct dynamic stiffness as the excitation frequency increases. That is, a lot of air volume content does as good a job as a fraction as low as 0.20. Note the air mass fractions are just below 1% and ~ 5 % for inlet GVF=0.2 and 0.6, respectively (see Table 3).

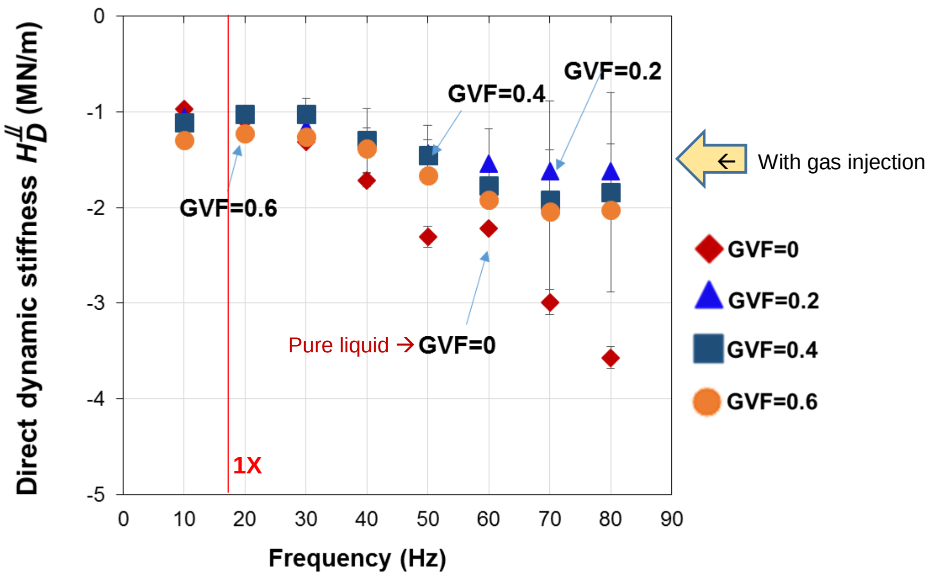

Fig. 23 Upstream Step Clearance Seal (USCS): direct dynamic stiffness versus frequency for seal supplied with air in oil mixture. Constant oil flow rate 7.6 L/min. Inlet GVF/supply pressure (bara): 0/2.38, 0.2/2.42, 0.4/2.43, 0.6/2.47. Shaft speed 1 krpm (ΩR=6.65 m/s or 16.7 Hz).

Table 3 lists the seal cross-coupled stiffness (k) and direct damping (C) coefficients for the upstream step clearance seal. The force coefficients are evaluated from dynamic load tests at a frequency (20 Hz), close to the shaft speed at 17 Hz (1 krpm). Note for all the test conditions, the whirl frequency ratio (WFR) is ~0.5, a typical magnitude for smooth annular seals. Air injection does not affect sensibly the seal stability indicator.

Table 3. Effect of gas volume content on the force coefficients of Upstream Step Clearance Seal (USCS): cross coupled stiffness (*k*), direct damping (*C*), and whirl frequency ratio (*k*/Ω*C*). Supply pressure varies to maintain same oil flow rate.

Pressure (bara)	Shaft speed (rpm)	Inlet GVF (-)	GMF (-)	k (kN/m)	C (kN-s/m)	WFR
1.80	1,000	0.0 oil only	0	921.7	17.4	0.50
2.38	"	0.0 ""	"	996.6	19.1	0.50
2.42	"	0.2	0.9 ‰	734.1	15.0	0.46
2.43	"	0.4	2.3 ‰	568.0	10.6	0.50
2.47	"	0.6	5.1 ‰	482.4	8.5	0.53
2.90	1,000	0.0 oil only	0	1124.0	22.0	0.49
2.90	3,500	0.0 ""	"	2914.0	16.4	0.48

On the stiffness hardening effect for an air in oil lubricated seal [25][6]

The experimental results show that a small gas content in the oil stream produces a significant change in the seals' dynamic stiffness *K* which hardens (increases) with excitation frequency. Recall that most liquids are hardly pure, i.e. without any gas content. The manufacturing process to produce commercial lubricants, for example, delivers a product with ~ 6% gas volume content.

The larger the seal centering stiffness, the larger its effect on a pump critical speed and its threshold speed of instability. Vertical electrical submersible pumps (ESPs) could use a higher K (>0) to ensure a statically stable unit. Incidentally, severe amplitude vibrations and apparent rotor instabilities in large (overhung) hydraulic turbine/pumps are not unusual [24]. These units show very low natural frequencies (a few Hz), and the rotor dynamic instability has a frequency above the operating shaft speed, i.e. a super synchronous speed event! In 1976 Ruud [26] reported a super synchronous vibration (3 to 7 Hz) in a massive vertical water pump (turning at just 2 Hz and successfully eliminated the shaft vibration by injecting air to the head covers and to the cavity formed by the outer surface of the blades and the casing. Later in 1996, Smith et al. [27] found a similar type of shaft vibration in a large water pump (speed of 5 Hz) whose natural frequency dropped from 12.5 Hz (dry condition) to 8.8 Hz when filled with water. Injecting air into the cavity behind the impeller removed the violent shaft excursions, super synchronous in character. The authors in Refs. [26, 27] do not provide an explanation on why air injection eliminated the severe shaft vibration issues.

How is it that a small content of gas[7] in a liquid stream produces such a significant change in (centering) stiffness?

Presently, BFM predictions help to elucidate the apparent odd behavior. For plain-seal # 1, Figure 24 depicts the direct dynamic stiffness $H_D^{\#}$ vs frequency for air/oil mixtures with an increasing gas content. With a pure oil, $H_D^{\#} = (K-\omega^2 M) < 0$ due to the large apparent mass of the liquid and a very low static stiffness (K) since the flow is laminar. Even a small content of air (GVF = 0.1) hardens $H_D^{\#}$ for all frequencies, $0 < \omega/\Omega < 1.5$. With an inlet GVF increasing to 20%, the direct dynamic stiffness ($H_D^{\#}$) keeps increasing at a certain frequency, as the thick (green) arrow in the graph shows.

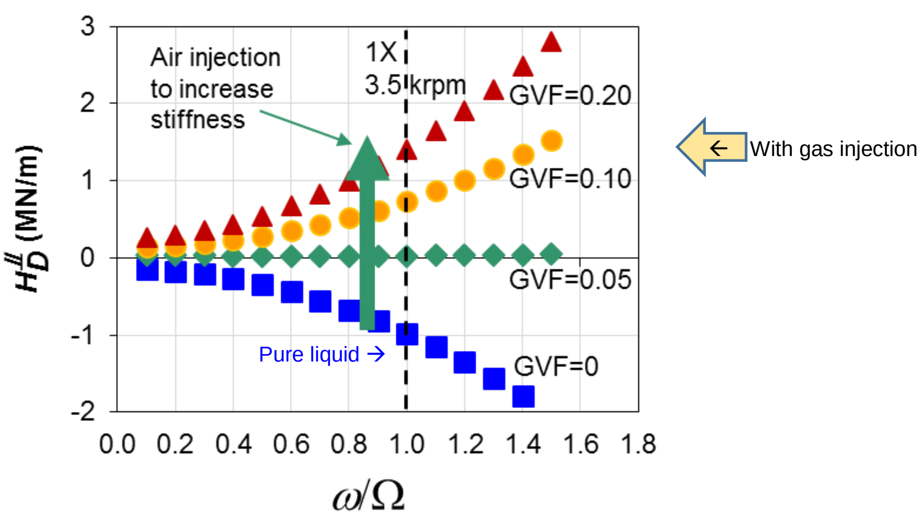

Fig. 24 Plain seal # 1: BFM predicted direct dynamic stiffness vs. frequency/shaft speed. Inlet GVF = 0 (liquid)**, 0.05, 0.1, and 0.2.** Pressure drop ΔP = 1.5 bar, rotor speed 3,500 RPM (58.3 Hz).

Recall the sound speed for pure oil (a_l) and air (a_g) are

$$a_l = \sqrt{\frac{\kappa}{\rho_l}} = 1{,}470 \text{ m/s}, \quad a_g = \sqrt{\gamma R T} = 353 \text{ m/s} \tag{12}$$

where κ = 1.79 GPa is the liquid bulk modulus and ρ_l=830 kg/m^3; while for air, R = 287 J/(kg·K), γ=1.4 and T= 310 K. The sound speed of a mixture (a) equals [28],

$$a^{-1} = \sqrt{\rho\left(\frac{\text{GVF}}{\rho_g a_g^2} + \frac{1-\text{GVF}}{\rho_l a_l^2}\right)} \tag{13}$$

where $\rho = \rho_g \cdot \text{GVF} + \rho_l \cdot (1-\text{GVF})$ is the mixture density.

6 This section paraphrases original material in Ref. [25] detailing a BFM analysis and computational fluid dynamics (CFD) predictions for *wet* seals. Both methods predict a direct dynamic stiffness that increases with frequency (ω) for operation with a gas in liquid two component flow.

7 Recall from Table 3, a 20% GVF corresponds to a gas mass fraction of just 0.9‰ at the seal inlet plane.

Figure 25 shows the (air in oil) mixture sound speed (normalized with respect to a_l versus GVF. Note that a GVF as small as 0.05, produces a 96% drop in sound speed, i.e. a=0.04 a_l. Such a low sound speed makes the mixture highly compressible; hence the stiffness hardens even at a low frequency excitation. The arrows in the graph show that as the flow proceeds through the seal its pressure drops and its GVF increases; and thus the sound speed of the mixture further drops while the mixture (axial) velocity increases. Note that the blue and red lines represent the sound speed change in seal#1, from the inlet plane to the outlet plane, for operation with inlet GVF=0.1 and 0.2, respectively (P_s=2.5 bara).

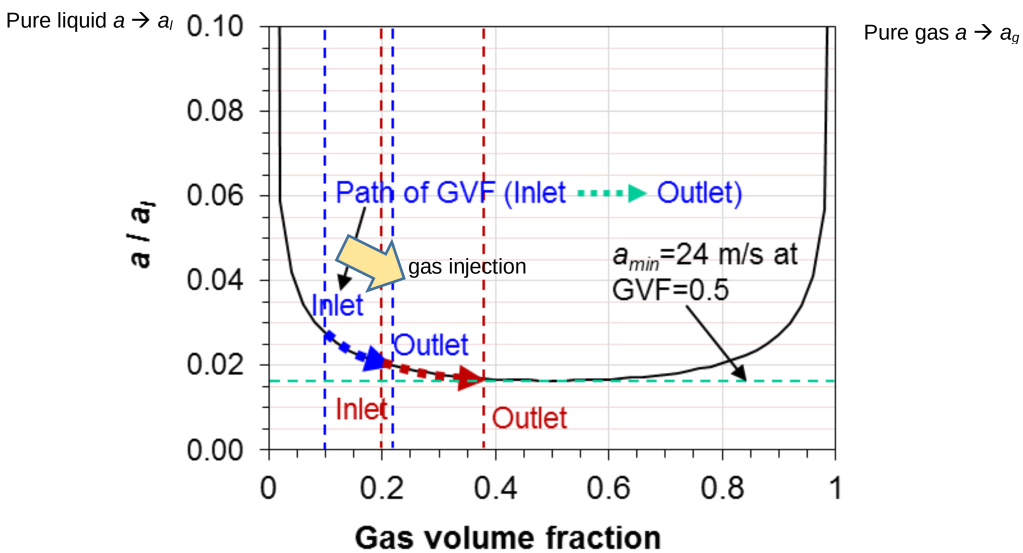

Fig. 25 Mixture sound speed (a/a_l) vs. gas volume fraction (GVF).
a_l = 1470 m/s (GVF = 0) and a_g = 353 m/s (GVF = 1) at 34 °C. Broken lines (blue and red) show the path of *sound speed for* GVF=0.1 and 0.2

CONCLUSIONS

In the subsea oil and gas industry, pumps must handle a range of flow conditions; all liquid at the start of well production, to a gas in liquid flow as the well depletes, to mostly slugs of gas content during (transient) operational upsets. Seals facing these stringent operating conditions show drastic changes in leakage, drag torque and power loss, and dynamic force coefficients, thus placing a penalty on the process efficiency and mechanical reliability and integrity of the turbomachine.

The lecture detailed comparisons of measured leakage and dynamic force coefficients for six annular seals supplied with an air in (thick) oil mixture ranging from just liquid to nearly just air. The physical properties of both oil liquid and air in the mixture are rather different. The seals tested include two uniform clearance seals differing in clearance, small and large; a third seal with a three-wave clearance profile; a fourth seal with a shallow groove pattern; and the last two seals with a step clearance, narrow to wide and wide to narrow). The extensive test campaign leads to the following knowledge.

1. For operation with a pure oil, the wavy seal shows slightly more leakage compared with the small clearance plain seal. The step clearance seal with the tightest clearance near the exit plane leaks the least. The grooved seal leaks more than the plain seals as the flow regime is laminar.
2. For operation with an air in oil mixture, the seal leakage, normalized with respect to the liquid only flow rate, decreases continuously as the GVF increases. The normalized leakages collapse into a single curve for the small uniform clearance seals and the three-wave seal. As the inlet GVF increases, the leakage of the grooved seal drops the fastest amongst the six seals.
3. The drag torque of the uniform (small) clearance seal decreases linearly with the GVF.
4. For operation with oil only (GVF=0), the six seals show frequency independent force coefficients (stiffness, damping and inertia). The three-wave seal shows a greater direct stiffness (K) compared with the K's for the two uniform clearance seals and the grooved seal. The upstream step narrow clearance seal shows K <0 that increases in magnitude with supply pressure (or flow); and the downstream step clearance seal reveals exactly the opposite effect, K > 0. A stepped clearance, narrow to wide, could easily produce a static instability in a vertical pump system, for example.
5. For operation with an air in oil mixture, the six seals produce frequency dependent force coefficients. The three-wave seal shows the largest dynamic stiffnesses (direct and cross coupled) and effective damping coefficient. The wavy seal *hardens* with frequency for operation with GVF as large as 0.9. The dynamic stiffness reduces with frequency quickly for the other seals.
6. Direct damping (C) for the uniform clearance seals and the three-wave seal reduce steadily (and proportionally) with GVF; the groove seal, on the other hand, shows C changing little with GVF ≤0.2.

7. The existing bulk flow model (BFM) predicts well the leakage and dynamic force coefficients for operation with pure oil and mixtures with a small gas content, GVF≤0.2. The discrepancy between prediction and test data grows as the gas content increases, GVF > 0.2.
8. The most significant impact of air injection, even a small fraction, is the hardening of a seal direct dynamic stiffness, and which could easily increase a pump system natural frequency well above its operating speed.
9. Air injection reduces simultaneously the direct damping (*C*) and cross coupled dynamic stiffness (*k*), hence the WRF remains at ~0.50.
10. Air injection into a liquid stream causes a dramatic reduction in the mixture sound speed to make it highly compressible; hence the hardening of the seal direct stiffness (or reduction of its added mass). This lecture provides physical rationale supporting a hitherto known practice in vertical pumps.

ACKNOWLEDGEMENTS

The authors thank the interest and financial support provided by the Texas A&M University Turbomachinery Research Consortium. We recognize Mr. Adrian D. Rangel, undergraduate student worker, for assisting to edit the videos. Thanks to Dr. Jing Yang, graduate student Mr. Tingcheng Wu, and Mr. Adrian Rangel for proofreading the lecture.

NOMENCLATURE

a_l, a_g	Sound speed in liquid and gas [m/s]
c	Seal radial clearance [m]
c_m	½ (c_{min}+ c_{max}), mean clearance of three-wave seal [m]
c_T, c_B	Top and bottom clearances in step clearance seal [m]
$C_{i,j}$	Damping coefficients [N.s/m], $i, j = X, Y$
C_S	Structure damping coefficient [N/m],
D	$D = 2R$, Journal diameter [m]
d_g, l_g, l_l	Groove depth and length, land length [m]
F_X, F_Y	Components of external excitation force [N]
$H = H_D^{//} + i\,H^{\perp}$	Seal complex dynamic stiffness [N/m]
$H_D^{//}$, $H_C^{//}$	Dynamic direct & cross-coupled stiffnesses [N/m]
$H^{\perp}$	ωC. Seal quadrature stiffness [N/m]
$K_{i,j}$	Stiffness coefficients[N/m], $i, j = X, Y$
K_S	Structure stiffness coefficient [N/m]
L	Seal length [mm]
L_T, L_B	Axial length of top clearance and bottom clearance in step clearance seal [m]
$\dot{m}_l, \dot{m}_g$	Mass flow rate for pure liquid and pure gas [kg/s]
$\dot{m}_m$	$\dot{m}_m = \dot{m}_l + \dot{m}_g$, Mass flow rate of air in oil mixture [kg/s]
$M_{i,j}$	Seal mass coefficients [N.s/m], $i, j = X, Y$
M_S	Structure mass coefficient [N/m],
N	Shaft rotational speed [rev/min]
P_a, P_s	Ambient pressure and supply pressure [Pa]
Q_l , Q_g	Flow rate for pure liquid and pure gas [m^3/s]
Q_m	Flow rate for two-phase mixture [m^3/s]
T	Torque [N·m]
X, Y	Seal cartridge displacements [m]
μ_l, μ_{ga}	Liquid and gas viscosities at ambient pressure and T = 37 ºC [Pa.s]
ρ_l, ρ_{ga}	Liquid and gas densities at ambient pressure and T = 37 ºC [kg/m^3]
ρ_m	Mixture or two-phase fluid density [kg/m^3]
Ω	N x(π/30). Shaft angular speed [rad/s]
ω	Excitation frequency [Hz]

MATRICES AND VECTORS

A	Absolute acceleration vector [m/s^2]
C	Damping matrix, $\mathbf{C} = \mathbf{C_S} + \mathbf{C_{seal}}$ [N·s/m]
F	External excitation force vector [N]
H	$\mathbf{K} - \omega^2\,\mathbf{M} + i\,\omega\,\mathbf{C}$. System complex dynamic stiffness matrix [N/m]
K	System stiffness matrix, $\mathbf{K} = \mathbf{K_S} + \mathbf{K_{seal}}$ [N/m]
Z	Seal cartridge displacement vector [m]

SUBSCRIPTS

m	Mixture or two component flow
g, l, pl	Gas and liquid, pure liquid
S	Structure
Seal	Seal

ABBREVIATIONS

BFM	Bulk flow model
GVF	Gas volume fraction
GMF	Gas mass fraction
LMF	Liquid mass fraction
LVF	Liquid volume fraction
OD	Outside diameter
ID	Inside diameter
SSV	Sub-synchronous vibration
USCS	Upstream step clearance seal
DSCS	Downstream step clearance seal
WFR	Whirl frequency ratio

REFERENCES

[1] San Andrés, L., Lu, X., and Zhu, J., 2018, "On the Leakage and Rotordynamic Force Coefficients of Pump Annular Seals Operating with Air/Oil Mixtures: Measurements and Predictions," *Proc. 2nd Asia Turbomachinery & Pump Symposium*, Singapore, Mar. 13-15.

[2] Black, H., 1969, "Effect of Hydraulic Forces on Annular Pressure Seals on the Vibrations of Centrifugal Pump Rotors," J. Mech. Eng. Sci., **11**(2), pp. 206-213.

[3] Childs, D.W., 2013, *Turbomachinery Rotordynamics with Case Studies*, Minter Spring Publishing, Wellborn, TX, Chap. 7. pp. 323-342.

[4] Childs, D.W., Norrbin, C.S., and Philips, S., 2014, "A Lateral Rotordynamics Primer on Electric Submersible Pumps (ESPs) for Deep Subsea Applications," *Proc.* 43rd *Turbomachinery* & 30th *Pump Symposia*, Houston, TX, Sept. 23-25.

[5] Amaike, M., Suzuki, T., Okafuji, K., Tashima, K., Tokoi, H., Nishihama, K., Suzuki, T., Sawahata, M., Peng, S., Arai, A., Katayama, and K., Matsushita, O., 2017, "Technology for Reducing the Environmental Impact of Motors and Improving Their Reliability," Hitachi Review, **66**(5), pp. 91-101.

[6] Marscher, W. D., 2016, "An End-User's Guide to Centrifugal Pump Rotordynamics," *Proc.* 45th *Turbomachinery* & 32nd *Pump Symposia*, Houston, TX, Sept. 12-15.

[7] San Andrés, L., 2010, *Modern Lubrication Theory*, "Annular Pressure (Damper) Seals," Notes 12, Texas A&M University Digital Libraries, http://hdl.handle.net/1969.1/93252 [Access date: Sept. 15, 2017]

[8] Zirkelback, N., and San Andrés, L., 1996, "Bulk-Flow Model for the Transition to Turbulence Regime in Annular Seals," Tribol. Trans., **39**(4), pp. 835-842.

[9] Hirs, G.G., 1973, "A Bulk-Flow Theory for Turbulence in Lubricant Films," J. of Lubrication Tech., **95**(2), pp. 137-145.

[10] Gong, H., Falcone, G., Teodoriu, C., and Morrison, G. L., 2012, "Comparison of Multiphase Pumping Technologies for Subsea and Downhole Applications," Oil and Gas Facilities, **1**(01), pp. 36-46.

[11] San Andrés, L., 2012, "Rotordynamic Force Coefficients of Bubbly Mixture Annular Pressure Seals," ASME J. Eng. Gas Turb. Power, **134**(2), p. 022503.

[12] Arghir, M., Zerarka, E., and Pieanu, G., 2011, "Rotordynamic Analysis of Textured Annular Seals with Multiphase (Bubbly) Flow," INCAS Bulletin, **3**(3), pp 3-13.

[13] Iwatsubo, T., and Nishino, T., 1993, "An Experimental Study on the Static and Dynamic Characteristics of Pump Annular Seals," *Proc.of the 7th Workshop on Rotordynamic Instability Problems in High Performance Turbomachinery*, College Station, TX, May 10–12, pp. 30-45. Available at http://turbolab.tamu.edu/re-sources/instability-workshops.

[14] Brenne, L., Bjorge, T., and Gilarranz, J., 2005, "Performance evaluation of a Centrifugal Compressor Operating under Wet Gas Conditions," *Proc.s of the* 34th *Turbomachinery Symposium*, Houston, TX, USA. Sept. 12-15.

[15] Vannini, G., Bertoneri, M., Del Vescovo, G., and Wilcox, M., 2014, "Centrifugal Compressor Rotordynamics in Wet Gas Conditions," *Proc. of the* 43th *Turbomachinery &* 30th *Pump Users Symposia*, Houston, TX, September 23-25.

[16] Vannini, G., Bertoneri, M., Nielsen, K.K., Ludiciani, P., and Stronach, R., 2016, "Experimental Results and Computational Fluid Dynamics Simulations of Labyrinth and Pocket Damper Seals for Wet Gas Compression," ASME J. Eng. Gas Turb. Power, **138**, p. 052501.

[17] Zhang, M., James E. Mclean Jr., and Childs, D., 2017 "Experimental Study of the Static and Dynamic Characteristics of a Long Smooth Seal with Two-Phase, Mainly-Air Mixtures," ASME J. Eng. Gas Turb. Power, **139**(12), 122504.

[18] San Andrés, L., Lu, X., and Liu, Q., 2016, "Measurements of Flow Rate and Force Coefficients in a Short-Length Annular Seal Supplied with a Liquid/Gas Mixture (Stationary Journal)," Tribol. Trans., **59** (4), pp. 758-767.

[19] San Andrés, L., and Lu, X., 2017, "Leakage, Drag Power and Rotordynamic Force Coefficients of an Air in Oil (Wet) Annular Seal," ASME J. Eng. Gas Turb. Power, **140**(1), p. 012505.

[20] San Andrés, L., 2010, *Modern Lubrication Theory*, "Notes 14. Experimental Identification of Bearing Force Coefficients," Texas A&M University Digital Libraries, http://hdl.handle.net/1969.1/93254. [Access date: Sept. 15, 2017]

[21] Lu, X., and San Andrés, L., 2018, "Leakage and Rotordynamic Force Coefficients of a Three-Wave (Air in Oil) Wet Annular Sea: Measurements and Predictions," ASME Paper No. GT2018-75200.

[22] Nordmann, R., Dietzen, F. J., Janson, W., Frei, A., and Florjancic, S., 1986, "Rotordynamic Coefficients and Leakage Flow of Parallel Grooved Seals and Smooth Seals," *Proc. of the 5th Workshop on Rotordynamic Instability Problems in High-Performance Turbomachinery*, College Station, TX, June 2-4, pp. 129–153. Available at http://turbolab.tamu.edu/resources/instability-workshops/.

[23] San Andrés, L., Wu, T., Maeda, H., and Tomoki, O., 2018, "A Computational Fluid Dynamics Modified Bulk Flow Analysis for Circumferentially Shallow Grooved Liquid Seals," ASME J. Eng. Gas Turb. Power, **140**(1), p. 012504.

[24] Nishimura, H., Horiguchi, H., Suzuki, T., Sugiyama, K., and Tsujimoto, Y., 2016, "Sub- and Super-Synchronous Self-Excited Vibrations of a Columnar Rotor Due to Axial Clearance Flow," 28th IAHR Symposium on Hydraulic Machinery and Systems, Grenoble, France, July 4-8.

[25] San Andrés, L., Yang J., and Lu, X., 2018, "On the Leakage, Torque and Dynamic Force Coefficients of an Air in Oil (Wet) Annular Seal: A CFD Analysis Anchored to Test Data," ASME Paper No. GT2018-77140.

[26] Ruud, F.O., 1976, "Vibration of Deriaz Pumps at Dos Amigos Pumping Plant," ASME J. Fluids Eng., December, **98**(4), pp. 674-679.

[27] Smith, D.R., Price, S.M., and Kunz, F.K., 1996, "Centrifugal Pump Vibration Caused by Supersynchronous Shaft Instability Use of Pumpout Vanes to Increase Pump Shaft Stability," Proc. 13th International Pump Users Symposium, Houston, TX, Mar. 5-7.

[28] Andrews, M. J., and O'Rourke, P. J., 1996, "The Multiphase Particle-in-Cell (MP-PIC) Method for Dense Particulate Flows," Int. J. Multiphase Flow, **22**(2), pp. 379–402.